

## Article

# Design, Synthesis, and Anti-Tyrosinase, Anti-Melanogenic, and Antioxidant Activities of Novel (Z)-3-Benzyl-5-benzylidene-2-thioxothiazolidin-4-one Analogs

Hyeon Seo Park <sup>1,†</sup>, Hee Jin Jung <sup>1,†</sup>, Hye Soo Park <sup>1</sup>, Hye Jin Kim <sup>1</sup>, Yujin Park <sup>2</sup>, Pusoon Chun <sup>3</sup>, Hae Young Chung <sup>4</sup> and Hyung Ryong Moon <sup>1,\*</sup>

- <sup>1</sup> Department of Manufacturing Pharmacy, College of Pharmacy and Research Institute for Drug Development, Pusan National University, Busan 46241, Republic of Korea; gustj6956@pusan.ac.kr (H.S.P.); hjjung2046@pusan.ac.kr (H.J.J.); hyesoo0713@pusan.ac.kr (H.S.P.); khj3358@pusan.ac.kr (H.J.K.)
- <sup>2</sup> Department of Medicinal Chemistry, New Drug Development Center, Daegu-Gyeongbuk Medical Innovation Foundation, Daegu 41061, Republic of Korea; pyj1016@kmedihub.re.kr
- <sup>3</sup> College of Pharmacy and Inje Institute of Pharmaceutical Sciences and Research, Inje University, Gimhae 50834, Republic of Korea; pusoon@inje.ac.kr
- <sup>4</sup> Department of Pharmacy, College of Pharmacy and Research Institute for Drug Development, Pusan National University, Busan 46241, Republic of Korea; hyjung@pusan.ac.kr
- \* Correspondence: mhr108@pusan.ac.kr; Tel.: +82-51-510-2815; Fax: +82-51-513-6754
- † These authors contributed equally to this work.

**Abstract:** To discover novel anti-melanogenic compounds with tyrosinase inhibitory activity, (Z)-3-benzyl-5-benzylidene-2-thioxothiazolidin-4-one ((Z)-BBTT) analogs **1–12**, designed based on the hybrid structure of a  $\beta$ -phenyl- $\alpha,\beta$ -unsaturated carbonyl motif and a 3-benzyl-2-thioxothiazolidin-4-one scaffold, were synthesized as novel tyrosinase inhibitors. Of the 12 analogs, 2 (**6** and **8**) showed mushroom tyrosinase inhibitory activity similar to that of kojic acid, a representative tyrosinase inhibitor, and 3 analogs (**1–3**) exhibited mushroom tyrosinase inhibitory activity that was more potent than that of kojic acid. In particular, analog **3** revealed highly potent inhibition with an  $IC_{50}$  value of 90 nM, which was 214 times lower than that of kojic acid ( $IC_{50}$  value = 19.22  $\mu$ M). A kinetic study using mushroom tyrosinase and analogs **1–3** and **6** demonstrated that these analogs were competitive inhibitors, which was further supported by in silico studies. Analogs **1** and **3** have strong anti-melanogenic potency in B16F10 mammalian cells owing to their anti-tyrosinase activity without perceptible cytotoxicity in melanoma cells (B16F10) and the main epidermal cells (HaCaT). Moreover, analog **3** exhibited strong antioxidant capacity, scavenging reactive oxygen species, 2,2'-azino-bis(3-ethylbenzothiazoline-6-sulfonic acid) cation radical, and 2,2-diphenyl-1-picrylhydrazyl radical, partially contributing to its anti-melanogenic effect. (Z)-BBTT analogs, including analog **3**, may be promising candidates for inhibiting melanin production.

**Keywords:** melanin; tyrosinase; B16F10 cells;  $\beta$ -phenyl- $\alpha,\beta$ -unsaturated carbonyl; (Z)-BBTT

Academic Editors: Maria Isabel L. Soares and Susana M. M. Lopes

Received: 26 December 2024

Revised: 22 January 2025

Accepted: 22 January 2025

Published: 23 January 2025

**Citation:** Park, H.S.; Jung, H.J.; Park, H.S.; Kim, H.J.; Park, Y.; Chun, P.; Chung, H.Y.; Moon, H.R. Design, Synthesis, and Anti-Tyrosinase, Anti-Melanogenic, and Antioxidant Activities of Novel (Z)-3-Benzyl-5-benzylidene-2-thioxothiazolidin-4-one Analogs. *Molecules* **2025**, *30*, 517. <https://doi.org/10.3390/molecules30030517>

**Copyright:** © 2025 by the authors.

Licensee MDPI, Basel, Switzerland.

This article is an open access article distributed under the terms and conditions of the Creative Commons Attribution (CC BY) license (<https://creativecommons.org/licenses/by/4.0/>).

## 1. Introduction

Ultraviolet (UV) rays are classified into UV-A (320–400 nm), UV-B (290–320 nm), and UV-C (200–290 nm), depending on wavelength [1]. UV-C, which has the highest energy and shortest wavelength, is blocked by the Earth's atmosphere, including the ozone layer,

and barely reaches the Earth's surface. By contrast, UV-A and UV-B, which have longer wavelengths, reach the Earth's surface and exert various effects on living organisms. In humans, UV-B is essential for the photolysis of 7-dehydrocholesterol in the skin for the synthesis of previtamin D3 [2,3]. Although UV rays can have positive effects on living organisms, they can destroy keratinocytes and fibroblasts in the epidermis and dermis, respectively, thereby causing wrinkles. Melanin, a polymer containing indole or thiazine rings, is produced in the skin upon UV radiation exposure. It has a chemical structure that absorbs or scatters UV rays, thus protecting the skin cells [4]. Indeed, melanin production is a defense mechanism of cells for protection against UV rays [5]. However, excessive melanin production in the skin can cause various cosmetic problems such as age spots, freckles, melasma, actinic keratosis, lentigines, skin hyperpigmentation diseases, and even skin cancer [6–8]. Therefore, the demand is continuous for the discovery of new and more effective anti-melanin ingredients for skin beauty and treatments related to skin hyperpigmentation.

Melanin is synthesized through various enzymatic and nonenzymatic reactions in melanosomes—organelles within melanocytes in the skin epidermis. Synthesized melanin is then transferred to the surrounding keratinocytes and is the most important factor in determining skin color [9]. In addition to neuromelanin, which exists in nerve cells, two types of melanin are found in humans. Eumelanin has a relatively dark color (black to brown), whereas pheomelanin has a relatively light color (yellow to red) [10,11]. These two melanins are biosynthesized from a common intermediate, dopaquinone. Pheomelanin is synthesized from dopaquinone solely through nonenzymatic chemical reactions, whereas eumelanin is synthesized through both nonenzymatic and enzymatic chemical reactions catalyzed by tyrosinase-related protein-1 (TRP-1), TRP-2, and tyrosinase [12]. Dopaquinone is synthesized from L-tyrosine via two sequential enzymatic oxidative reactions. These processes are rate-limiting steps, and the two oxidation reactions are catalyzed by the same enzyme, tyrosinase. Although several strategies can inhibit melanin production, tyrosinase inhibition is the most studied and is recognized as the most effective method because it participates in the rate-limiting step of melanin biosynthesis. Tyrosinase oxidizes L-tyrosine to L-DOPA through monophenolase activity and subsequently oxidizes L-DOPA to dopaquinone through diphenolase activity [13–15]. Dopaquinone is converted to pheomelanin in the presence of thiol compounds such as cysteine or to dopachrome through an intramolecular auto-reaction and then to eumelanin through several consecutive reactions [12,16]. Dopaquinone is very rapidly converted into dopachrome, which can strongly absorb light at 475 nm. Thus, a widely used method to assess the effect of a compound on tyrosinase activity is to measure its absorbance at 475 nm [17].

Compounds containing 3-benzyl-2-thioxothiazolidin-4-one have exhibited a variety of biological activities, including antiviral [18], anticancer [19], antibacterial [20], glycogen synthase kinase 3 inhibition [21], urease inhibition [22], anti-inflammatory [23], antituberculosis [24], and antifungal [20] activities. The  $\beta$ -phenyl- $\alpha,\beta$ -unsaturated carbonyl (PUSC) motif was confirmed to act as an important chemical skeleton of tyrosinase inhibitors (Figure 1). In particular, when the phenyl moiety of the PUSC motif has a hydroxyl substituent at both positions 2 and 4, the compound has good tyrosinase inhibitory activity [25–29]. Topical skin-whitening agents would be advantageous if they are slightly hydrophobic, allowing them to be easily absorbed into the skin. Therefore, to synthesize novel PUSC-type tyrosinase inhibitors with hydrophobic properties, lipophilic 3-benzyl-2-thioxothiazolidin-4-one was designed as an active methylene compound that reacts with various benzaldehydes, and (*Z*)-3-benzyl-5-benzylidene-2-thioxothiazolidin-4-one ((*Z*)-BBTT) analogs **1–12** were synthesized as the final target compounds (Figure 1). The ability of (*Z*)-BBTT analogs to inhibit tyrosinases was investigated in mushroom and murine cells, and

their capacity to inhibit melanin production was examined in murine cells. Additionally, antioxidant activity of these analogs was evaluated by their potency to remove 2,2'-azino-bis(3-ethylbenzothiazoline-6-sulfonic acid) cation (ABTS<sup>+</sup>) radical, 2,2-diphenyl-1-picrylhydrazyl (DPPH) radical, and reactive oxygen species (ROS). Moreover, the tyrosinase inhibitory mode of action of (Z)-BBTT analogs and the chemical interactions between tyrosinase and these analogs were examined.

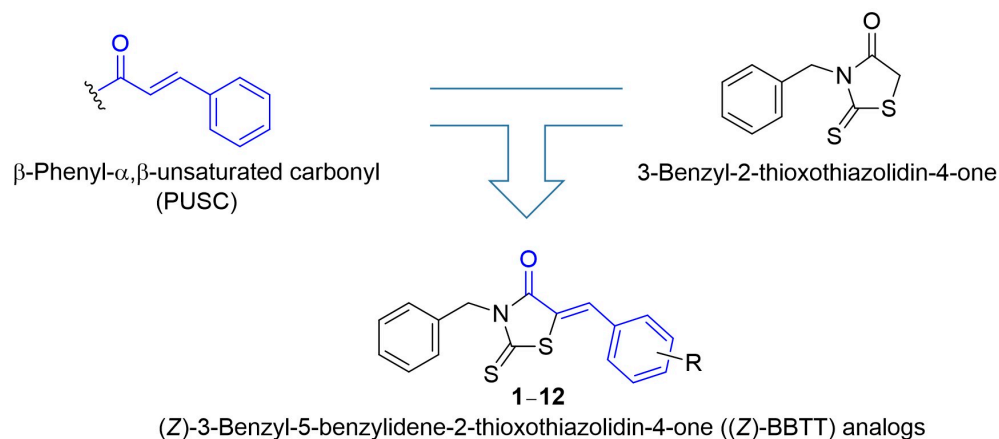
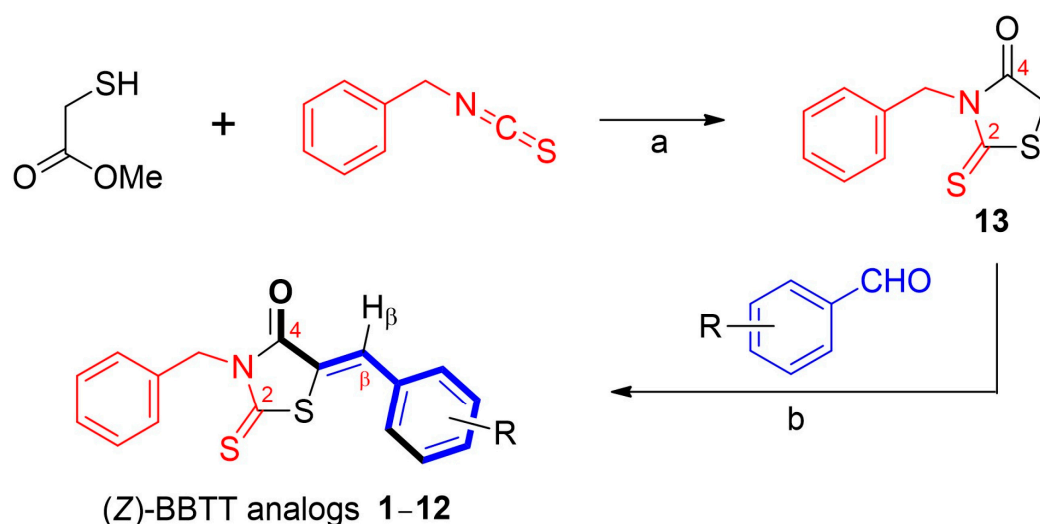


**Figure 1.** Chemical structures of  $\beta$ -phenyl- $\alpha,\beta$ -unsaturated carbonyl (PUSC) and lipophilic 3-benzyl-2-thioxothiazolidin-4-one, and the final target compounds, (Z)-3-benzyl-5-benzylidene-2-thioxothiazolidin-4-one ((Z)-BBTT) analogs created by the structural hybrid of PUSC and 3-benzyl-2-thioxothiazolidin-4-one.

## 2. Results and Discussion

### 2.1. Synthesis of Target Compounds (Z)-BBTT Analogs 1–12

To synthesize the target compounds ((Z)-BBTT analogs 1–12), 3-benzyl-2-thioxothiazolidin-4-one (**13**) was used as a key intermediate for condensation with various benzaldehydes (Scheme 1). Compound **13** was prepared via the condensation of benzyl isothiocyanate and methyl 2-mercaptoacetate in the presence of trimethylamine in dichloromethane. Purification of **13** was performed by filtration and then washing with diethyl ether and hexane to remove impurities. In the <sup>13</sup>C nuclear magnetic resonance (NMR) spectrum, the C2 and C4 peaks of **13** appeared at 201.1 and 174.0 ppm, respectively, confirming the construction of a 2-thioxothiazolidin-4-one ring. The synthesis of final target analogs 1–12 was achieved using a Knoevenagel condensation reaction: the reflux of **13** and twelve benzaldehydes (1.0 equiv.) with various substituents in the presence of sodium acetate (6.0 equiv.) in acetic acid. Purification of 1–12 was performed by filtration and then washing with dichloromethane and hexane to remove impurities. The synthetic yields ranged from 47% to 92%. The trisubstituted alkenes generated by the Knoevenagel condensation reaction were (Z)-isomers. There is a paper that reported obtaining (Z)-isomers through a Knoevenagel condensation reaction of **13** and various benzaldehydes [19]. (Z)-isomers have less steric hindrance than the corresponding (E)-isomers and are thermodynamically more stable than the latter owing to intramolecular H-bonding between the carbonyl oxygen and vinylic H (H<sub>β</sub>). In addition, the <sup>3</sup>J<sub>C4-Hβ</sub> values of C4 obtained in a proton-coupled <sup>13</sup>C-mode NMR indicated that the trisubstituted exocyclic methylene geometry is (Z)-stereochemistry. Vogeli et al. reported that the <sup>3</sup>J<sub>C4-Hβ</sub> is 3.5–7.0 Hz when the carbonyl and β-H in trisubstituted alkenes of  $\alpha,\beta$ -unsaturated carbonyl compounds are on the same side and is generally  $\geq 10$  Hz when they are on opposite sides [30]. The C4 peak of analog **3** appeared as a doublet (5.8 Hz) of triplets (2.9 Hz) owing to coupling by protons of β-H and N-CH<sub>2</sub>, indicating that the carbonyl and β-H are on the same side.



**Scheme 1.** Synthetic scheme of (*Z*)-3-benzyl-5-benzylidene-2-thioxothiazolidin-4-one ((*Z*)-BBTT) analogs **1–12**. The reagents and conditions were as follows: (a) Et<sub>3</sub>N, CH<sub>2</sub>Cl<sub>2</sub>, RT, 3.5 h, and 94% and (b) NaOAc, AcOH, reflux, 2–4 h, and 47–92%.

## 2.2. Inhibitory Activity of (*Z*)-BBTT Analogs 1–12 Against Mushroom Tyrosinase

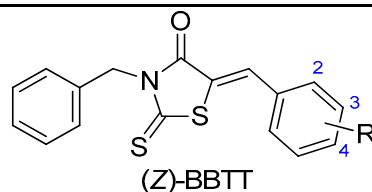
The mushroom tyrosinase inhibitory activity of (*Z*)-BBTT analogs **1–12** was evaluated in the presence of two substrates, L-tyrosine and L-DOPA, by measuring the optical density of the generated dopachrome at 475 nm. Kojic acid, a well-known tyrosinase inhibitor, was used as a standard to compare the inhibitory activity.

The tyrosinase inhibitory activities of the (*Z*)-BBTT analogs were assessed in the presence of L-tyrosine. Kojic acid revealed an IC<sub>50</sub> value of 19.22 μM, and two (*Z*)-BBTT analogs, **6** with 4-methoxyphenyl and **8** with 2,4-dimethoxyphenyl, showed potent mushroom tyrosinase inhibitory activity similar to that of kojic acid (IC<sub>50</sub> values of **6** and **8**: 19.11 and 18.57 μM, respectively) (Table 1). In contrast, analog **7** (IC<sub>50</sub> value: 56.19 μM) containing 3,4-dimethoxyphenyl inhibited tyrosinase activity to a lesser extent than kojic acid. (*Z*)-BBTT analogs **1–3**, which have only hydroxyl substituents on the β-phenyl ring of (*Z*)-BBTT analogs, exhibited a stronger tyrosinase inhibitory effect compared with kojic acid. Analog **1** with 4-hydroxyphenyl had an IC<sub>50</sub> value of 4.69 μM, which was four-fold lower than that of kojic acid. Insertion of an additional hydroxyl substituent into position 3 of the β-phenyl ring in **1** did not affect the tyrosinase inhibitory effect (IC<sub>50</sub> value of **2** with 3,4-dihydroxyphenyl: 5.75 μM). However, insertion of an additional hydroxyl substituent into position 2 of the β-phenyl ring in **1** greatly increased the tyrosinase inhibitory activity (IC<sub>50</sub> value of **3** with 2,4-dihydroxyphenyl: 0.09 μM). The inhibitory potency of analog **3** was 52 and 214 times stronger than that of analog **1** and kojic acid, respectively. Meanwhile, three analogs (**4**, **5**, and **11**) with one hydroxyl substituent and one methoxyl or bromo substituent exhibited slightly lower tyrosinase inhibitory activity than kojic acid (IC<sub>50</sub> values of **4** with 4-hydroxy-3-methoxyphenyl, **5** with 3-hydroxy-4-methoxyphenyl, and **11** with 3-bromo-4-hydroxyphenyl: 45.52, 39.01, and 66.26 μM, respectively). Analog **9** containing trimethoxyphenyl and analogs **10** and **12** containing hydroxyl surrounded by two methoxyl or bromo groups on the β-phenyl ring had IC<sub>50</sub> values > 200 μM.

In addition, the tyrosinase inhibitory activity of the (*Z*)-BBTT analogs was assessed in the presence of L-DOPA. Most analogs showed lower mushroom tyrosinase inhibitory activity when using the L-DOPA substrate than when using the L-tyrosine substrate (Table 1). An exception was analog **9**, containing 3,4,5-trimethoxyphenyl, which exhibited stronger tyrosinase inhibitory activity in the presence of L-DOPA than in the presence of

L-tyrosine ( $IC_{50}$  values of **9**: 97.23  $\mu\text{M}$  in the presence of L-DOPA vs. >200  $\mu\text{M}$  in the presence of L-tyrosine). Kojic acid showed tyrosinase inhibitory potency with an  $IC_{50}$  value of 26.54  $\mu\text{M}$ . Analogs **1**, **2**, and **6** showed potent tyrosinase inhibitory activity either similar to or slightly weaker than that of kojic acid ( $IC_{50}$  values of **1** with 4-hydroxyphenyl, **2** with 3,4-dihydroxyphenyl, and **6** with 4-methoxyphenyl: 38.10, 27.47, and 33.54  $\mu\text{M}$ , respectively). Similar to that in the presence of L-tyrosine, analogs **2** and **3**, which contain two hydroxyl substituents on the  $\beta$ -phenyl ring, showed differences in tyrosinase inhibition depending on the relative position of the two hydroxyls. Analog **2** with 3,4-dihydroxyphenyl demonstrated tyrosinase inhibitory activity similar to that of kojic acid. Meanwhile, analog **3** with 2,4-dihydroxyphenyl showed notably more potent tyrosinase inhibitory activity compared with kojic acid, with approximately 100 times greater potency ( $IC_{50}$  value: 0.27  $\mu\text{M}$ ) than kojic acid. Analogs **7** and **8**, obtained by replacing the hydroxyls in analogs **2** and **3** with methoxyls, decreased the tyrosinase inhibitory activity ( $IC_{50}$  values of **7** with 3,4-dimethoxyphenyl and **8** with 2,4-dimethoxyphenyl were 70.64 and 51.14  $\mu\text{M}$ , respectively). Analogs **4**, **5**, and **11**, which have one hydroxyl substituent and one methoxyl or bromo substituent, showed moderate tyrosinase inhibitory effects, with  $IC_{50}$  values ranging from 90.01 to 121.24  $\mu\text{M}$ . By contrast, analogs **10** and **12**, which have one hydroxyl substituent and two methoxyl or bromo substituents, exhibited tyrosinase inhibitory activity with  $IC_{50}$  values > 200  $\mu\text{M}$ , as observed in the presence of L-tyrosine.

**Table 1.** Mushroom tyrosinase inhibitory activity of (Z)-3-benzyl-5-benzylidene-2-thioxothiazolidin-4-one ((Z)-BBTT) analogs **1–12** in the presence of its substrates L-tyrosine and L-DOPA.



Compound	R	$IC_{50}$ ( $\mu\text{M}$ )	
		L-Tyrosine	L-Dopa
<sup>a</sup> Kojic acid		19.22 $\pm$ 1.29	26.54 $\pm$ 0.17
<b>1</b>	4-Hydroxy	4.69 $\pm$ 0.58	38.10 $\pm$ 2.26
<b>2</b>	3,4-Dihydroxy	5.75 $\pm$ 0.81	27.47 $\pm$ 1.84
<b>3</b>	2,4-Dihydroxy	0.09 $\pm$ 0.01	0.27 $\pm$ 0.04
<b>4</b>	4-Hydroxy-3-methoxy	45.52 $\pm$ 2.49	121.24 $\pm$ 4.90
<b>5</b>	3-Hydroxy-4-methoxy	39.01 $\pm$ 2.15	91.01 $\pm$ 8.55
<b>6</b>	4-Methoxy	19.11 $\pm$ 2.03	33.54 $\pm$ 0.30
<b>7</b>	3,4-Dimethoxy	56.19 $\pm$ 1.98	70.64 $\pm$ 1.25
<b>8</b>	2,4-Dimethoxy	18.57 $\pm$ 1.23	51.14 $\pm$ 2.05
<b>9</b>	3,4,5-Trimethoxy	>200	97.23 $\pm$ 7.73
<b>10</b>	4-Hydroxy-3,5-dimethoxy	>200	>200
<b>11</b>	3-Bromo-4-hydroxy	66.26 $\pm$ 2.11	114.88 $\pm$ 2.28
<b>12</b>	3,5-Dibromo-4-hydroxy	>200	>200

<sup>a</sup> Kojic acid was used as a standard for comparing inhibitory activity.

Table 2 shows that when a hydroxyl substituent was positioned at  $R^4$  in the (Z)-BBTT structure, the addition of an additional hydroxyl substituent at  $R^2$  and  $R^3$  significantly and slightly increased the tyrosinase inhibitory activity, respectively. However, when a methoxyl substituent was positioned at  $R^4$ , the insertion of an additional hydroxyl substituent at  $R^3$  decreased the tyrosinase inhibitory activity. In the presence of L-tyrosine, the introduction of a hydroxyl substituent at  $R^4$  resulted in a greater tyrosinase inhibitory effect

than the introduction of a methoxyl substituent. However, in the presence of L-DOPA, these two substituents showed similar tyrosinase inhibitory activities.

**Table 2.** Structure–activity relationship between substitutions on the  $\beta$ -phenyl ring of (Z)-BBTT analogs and tyrosinase inhibition activity.

(Z)-BBTT analogs

Substitution	<sup>a</sup> Tyrosinase Inhibition
<span style="color: red;">R<sup>2</sup></span> = OH	<span style="color: red;">↑↑↑↑</span> when R <sup>4</sup> = OH
R <sup>3</sup> = OH	<span style="color: blue;">↓↓</span> when R <sup>4</sup> = OMe <span style="color: red;">↑</span> when R <sup>4</sup> = OH
<span style="color: blue;">R<sup>4</sup></span>	OH > MeO in the presence of L-tyrosine OH ≈ MeO in the presence of L-dopa

<sup>a</sup> Red and blue arrows represent increases and decreases in tyrosinase inhibitory activity, respectively. More arrows indicate stronger effects.

### 2.3. Kinetic Analysis of Mushroom Tyrosinase Using Lineweaver–Burk Plots

As analogs **1–3** and **6** had potent inhibitory activity against mushroom tyrosinase, their inhibitory mechanisms were investigated by measuring the initial formation rate of dopachrome in the presence of L-DOPA. Analogs were used at 0, 20, 40, and 80  $\mu\text{M}$  for **1**; 0, 15, 30, and 60  $\mu\text{M}$  for **2**; 0, 0.1, 0.2, and 0.4  $\mu\text{M}$  for **3**; and 0, 12.5, 25, and 50  $\mu\text{M}$  for **6**. L-DOPA was used at concentrations of 1, 2, 4, 8, and 16 mM.

The four Lineweaver–Burk plots for **1–3** and **6** are shown in Figure 2. All Lineweaver–Burk plots had four lines with different slopes and merged at one point on the y-axis, indicating that all analogs were competitive inhibitors that bound to the tyrosinase active site and competed with the substrates L-DOPA and L-tyrosine.



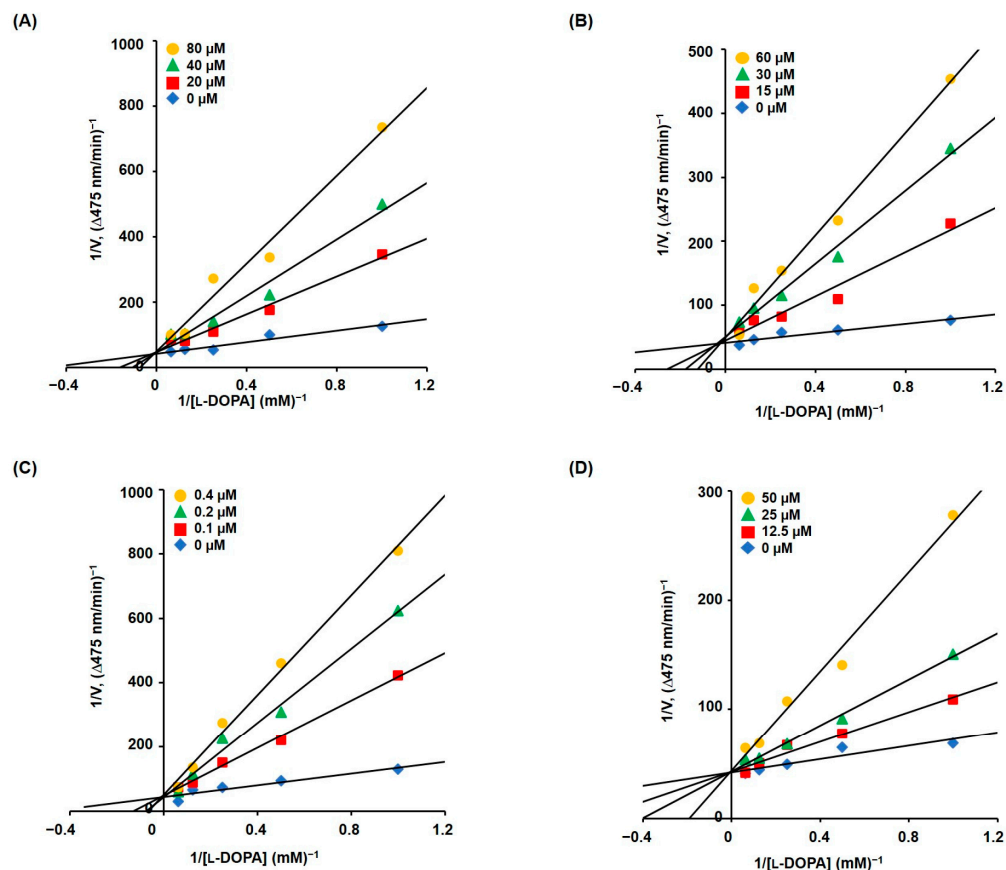


**Figure 2.** Lineweaver–Burk plots for **1–3** (A–C) and **6** (D) obtained by measuring the initial dopachrome production rate in the presence of various L-DOPA concentrations (1, 2, 4, 8, and 16 mM) using mushroom tyrosinase. The concentrations of the test analogs were 0, 20, 40, and 80  $\mu\text{M}$  for **1**; 0, 15, 30, and 60  $\mu\text{M}$  for **2**; 0, 0.1, 0.2, and 0.4  $\mu\text{M}$  for **3**; and 0, 12.5, 25, and 50  $\mu\text{M}$  for **6**.

To determine the inhibition constant ( $K_i$ ), Lineweaver–Burk plots for analogs **1–3** and **6** were converted to the corresponding Dixon plots by plotting the analog concentrations against the inverse of the initial dopachrome production rate. Each Dixon plot provided a picture of four straight lines that merged at one point in the second quadrant (Figure 3). The absolute value of the x-coordinate of the merged point is the  $K_i$  value. The  $K_i$  values for analogs **1–3** and **6** were 15.5, 12.2, 0.064, and 15.5  $\mu\text{M}$ , respectively, indicating that analog **3** had the greatest binding affinity with tyrosinase among the analogs.

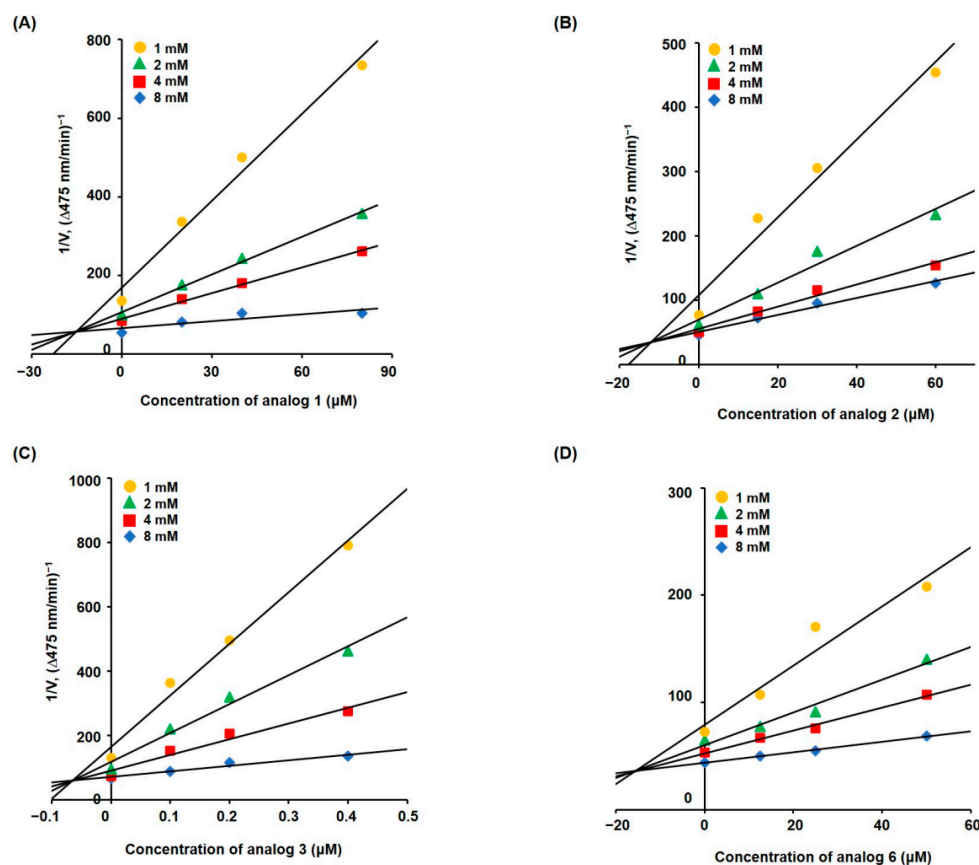


**Figure 3.** Dixon plots for analogs 1–3 (A–C) and 6 (D) obtained by converting Lineweaver–Burk plots. The concentrations of the test analogs were 0, 20, 40, and 80  $\mu\text{M}$  for 1; 0, 15, 30, and 60  $\mu\text{M}$  for 2; 0, 0.1, 0.2, and 0.4  $\mu\text{M}$  for 3; and 0, 12.5, 25, and 50  $\mu\text{M}$  for 6. L-DOPA was used at concentrations of 1, 2, 4, and 8 mM.

#### 2.4. In Silico Docking Simulation of (Z)-BBTT Analogs and Mushroom Tyrosinase

Docking simulations with mushroom tyrosinase were performed for analogs 1–3 and 6, which showed excellent inhibitory activities against mushroom tyrosinase. Kojic acid and AutoDock Vina 1.2.0 were used as the positive control and docking simulation software, respectively. To obtain information on the chemical interactions between tyrosinase amino acid residues and ligands (analogs 1–3 and 6 and kojic acid), LigandScout 4.4.8 (Inte: Ligand GmbH, Vienna, Austria) was used.

Figure 4 shows the docking simulation results. All docked compounds bound to the tyrosinase active site. Kojic acid participated in hydrogen bonding (H–B) of the 2-hydroxymethyl with Asn260 as an H–B donor and in pi–pi stacking of the pyran-4-one with His263, providing a binding energy of  $-5.4$  kcal/mol. Analog 1 participated in one H–B of the 4-hydroxy group with Asn81 as an H–B acceptor and in hydrophobic interactions of the  $\beta$ -phenyl and benzyl rings with Val283, providing a binding energy of  $-7.5$  kcal/mol. Analog 2 formed two hydrogen bonds between the 3-hydroxy moiety and two amino acids (Glu322 and His85) and participated in hydrophobic interactions between the  $\beta$ -phenyl and benzyl rings and amino acids (Val283 and Ala286). These chemical interactions contributed to a binding energy of  $-7.8$  kcal/mol. Each hydroxyl substituent of analog 3 created an H–B: the 2-hydroxyl substituent that interacted with Glu322 and the 4-hydroxyl substituent that interacted with Cys83. Additionally, analog 3 generated hydrophobic interactions between the  $\beta$ -phenyl ring and Val283 and between the benzyl ring and two amino acids (Val283 and Phe264). These chemical interactions provided a binding energy of  $-7.8$  kcal/mol. Analog 6 only formed hydrophobic interactions between the  $\beta$ -



phenyl and benzyl rings and amino acids (Val283, Phe264, and Ala286), providing  $-7.6$  kcal/mol binding energy. All four (*Z*)-BBTT analogs showed stronger binding affinities than kojic acid. Val283 participated in hydrophobic interactions with all (*Z*)-BBTT analogs, implying that Val283 acts as an important amino acid in the inhibition of tyrosinase activity by (*Z*)-BBTT analogs. Glu322 participated in the formation of H-Bs with analogs 2 and 3, suggesting that Glu322 is also a key amino acid that exerts a tyrosinase inhibitory effect.

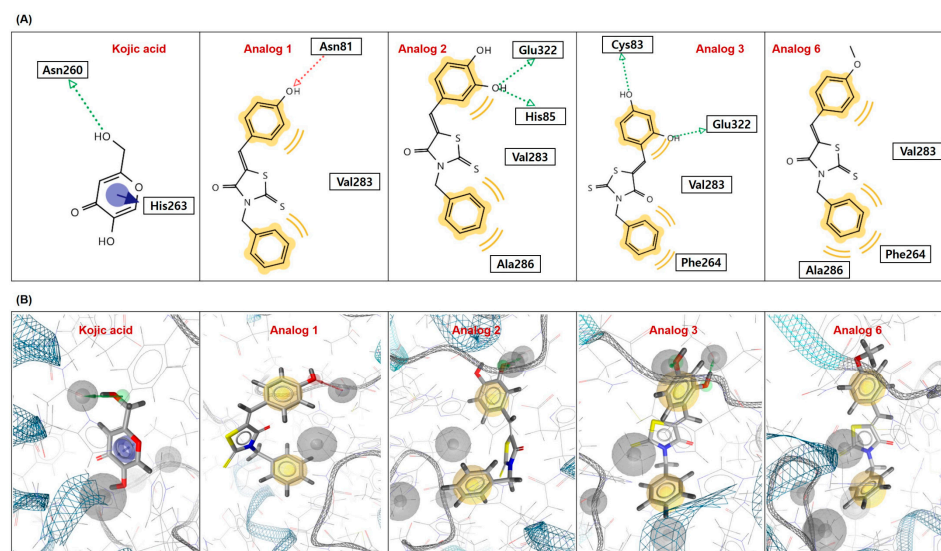


**Figure 4.** Chemical interactions between tyrosinase and ligands (kojic acid [positive control] and analogs 1–3 and 6) obtained from LigandScout after docking simulation using AutoDock Vina. (A) Two- and (B) three-dimensional pictures. Blue arrow, pi–pi stacking; yellow wave, hydrophobic interaction; green arrow, hydrogen bonding (H–B donor from the ligand’s perspective); and red arrow, hydrogen bonding (H–B acceptor from the ligand’s perspective). (B) In molecules, red, blue, and yellow represent oxygen, nitrogen, and sulfur, respectively.

### 2.5. Cell Viability of (*Z*)-BBTT Analogs on B16F10 Cells

Because (*Z*)-BBTT analogs 1–3 exhibited significant mushroom tyrosinase inhibitory activity, the cell viability for these analogs was assessed prior to investigating their cellular tyrosinase activity and ability to inhibit melanin production in B16F10 cells. Cell viability for analogs 1–3 was examined on B16F10 cells at 1, 2, 5, and 10  $\mu\text{M}$  concentrations for 72 h.

The cytotoxicity results are shown in Figure 5. Analog 2 was cytotoxic at all tested concentrations, whereas analogs 1 and 3 were not cytotoxic to B16F10 cells up to 10  $\mu\text{M}$ , which is the highest tested concentration. Thus, analogs 1 and 3 were used at concentrations  $\leq 10$   $\mu\text{M}$  in B16F10-cell-based experiments measuring melanin contents and cellular tyrosinase activity.

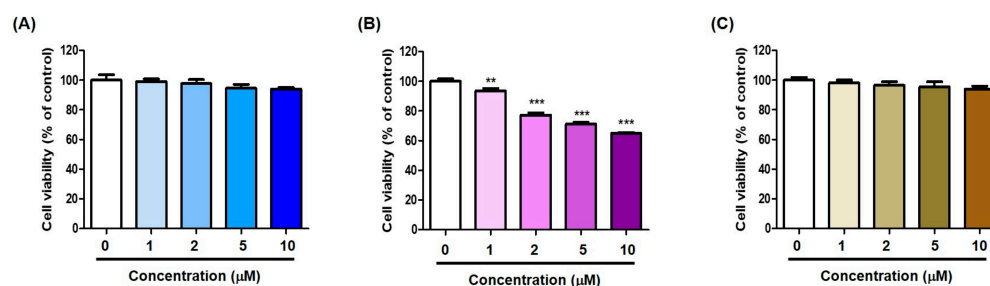


**Figure 5.** B16F10 cell viability in the presence of (*Z*)-3-benzyl-5-benzylidene-2-thioxothiazolidin-4-one analogs 1 (A), 2 (B), and 3 (C). \*\*\*  $p < 0.001$  and \*\*  $p < 0.01$  vs. the nontreated group.

## 2.6. Effect of (Z)-BBTT Analogs 1 and 3 on Melanin Production in B16F10 Cells

The effects of analogs **1** and **3** on melanin production were examined in B16F10 cells using kojic acid as a positive control. The analogs were administered at concentrations of 2, 5, and 10  $\mu\text{M}$ , and kojic acid was used at 10  $\mu\text{M}$ . Stimulators comprising 1  $\mu\text{M}$   $\alpha$ -melanocyte-stimulating hormone ( $\alpha$ -MSH) and 200  $\mu\text{M}$  3-isobutyl-1-methylxanthine (IBMX) were administered 1 h after test sample treatment. The effects of analogs **1** and **3** on melanin production were determined by measuring the optical density at 405 nm after 72 h of treatment.

Treatment with stimulators largely increased melanin contents (5.0-fold increase), and exposure to kojic acid significantly reduced the stimulator-induced increased melanin content by 4.0-fold (Figure 6). Analogs **1** and **3** significantly decreased the stimulator-induced increase in melanin contents in a concentration-dependent manner. Analog **1** showed a slightly more potent anti-melanogenic effect than analog **3**. Analog **1** at 2  $\mu\text{M}$  reduced melanin content to levels similar to that of 10  $\mu\text{M}$  kojic acid, and at 10  $\mu\text{M}$ , it decreased the stimulator-induced melanin contents by 1.9-fold. Analog **3** at 2  $\mu\text{M}$  inhibited melanin production more weakly than 10  $\mu\text{M}$  kojic acid, although it inhibited melanin production significantly more potently than kojic acid at the same concentration (10  $\mu\text{M}$ ).

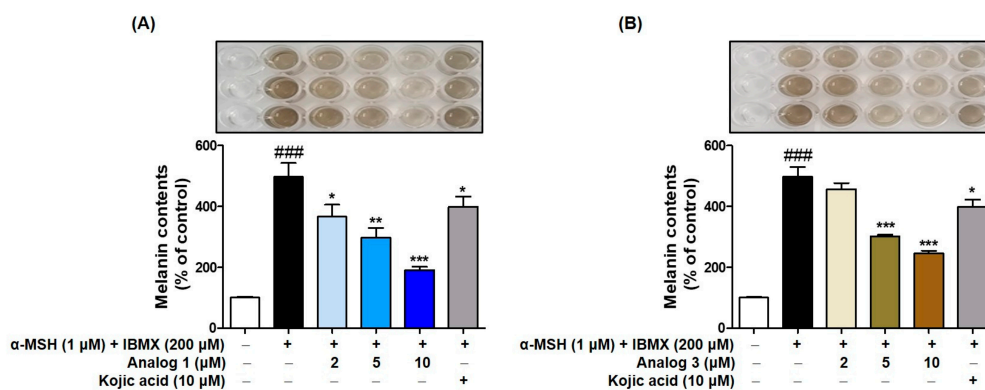


**Figure 6.** Effect of analogs **1** (A) and **3** (B) on melanin production in B16F10 cells. Stimulators  $\alpha$ -MSH and IBMX were treated at 1 and 200  $\mu\text{M}$ , respectively, 1 h after treatment of analogs (2, 5, and 10  $\mu\text{M}$ ). After 72 h, melanin contents were determined by measuring the optical density at 405 nm. Kojic acid was used as a positive control.  $\alpha$ -MSH,  $\alpha$ -melanocyte-stimulating hormone; IBMX, 3-isobutyl-1-methylxanthine. \*\*\*  $p < 0.001$ , \*\*  $p < 0.01$ , and \*  $p < 0.05$  vs. stimulator-treated group; ###  $p < 0.001$  vs. untreated control.

## 2.7. Effect of (Z)-BBTT Analogs 1 and 3 on Tyrosinase Activity in B16F10 Cells

To examine whether the anti-melanogenic effects of analogs **1** and **3** observed in Figure 6 were attributable to their ability to inhibit B16F10 cellular tyrosinase activity, the effects of analogs **1** and **3** on cellular tyrosinase activity were assessed in B16F10 cells. Similar to that in the melanin content experiments, kojic acid (10  $\mu\text{M}$ ) was used as a positive control. B16F10 cells were pretreated with an analog (**1** and **3**) at 2, 5, and 10  $\mu\text{M}$  or kojic acid and then exposed to stimulators (1  $\mu\text{M}$   $\alpha$ -MSH and 200  $\mu\text{M}$  IBMX) 1 h later. The cellular tyrosinase inhibitory activity of the test samples was determined by measuring their optical density at 475 nm 72 h after test sample treatment.

Stimulator treatment enhanced cellular tyrosinase activity by 3.4-fold compared with that in the control group (100%) (Figure 7). However, kojic acid exposure greatly reduced the stimulator-enhanced cellular tyrosinase activity by 2.4-fold. Treatment with analogs **1** and **3** also significantly decreased the stimulator-enhanced cellular tyrosinase activity in a concentration-dependent manner. At 10  $\mu\text{M}$ , both analogs **1** and **3** inhibited cellular tyrosinase activity more strongly than kojic acid. The pattern of cellular tyrosinase inhibition

was similar to that of melanogenesis inhibition, indicating that the anti-melanogenic effect of (Z)-BBTT analogs **1** and **3** was primarily attributable to their ability to inhibit tyrosinase activity.

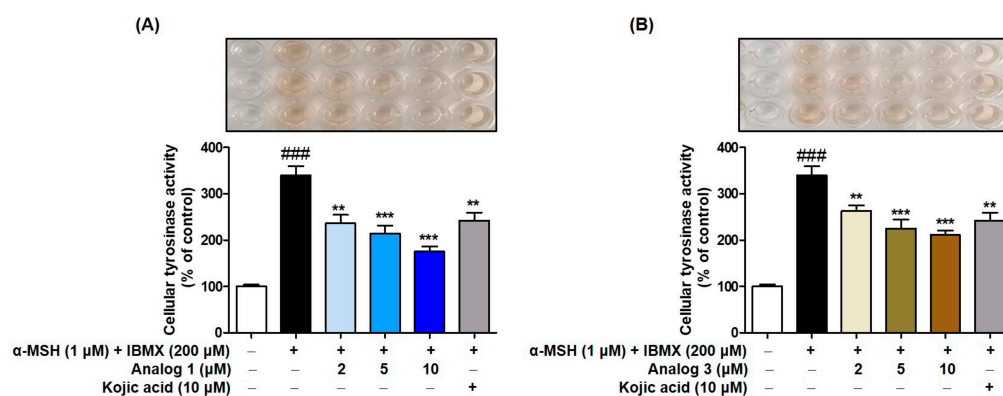


**Figure 7.** Effects of analogs **1** (A) and **3** (B) on B16F10 cellular tyrosinase activity. Stimulators  $\alpha$ -MSH and IBMX were treated at 1 and 200  $\mu$ M, respectively, 1 h after treatment of analogs (2, 5, and 10  $\mu$ M). After 72 h, tyrosinase activity was determined by measuring optical density at 475 nm.  $\alpha$ -MSH,  $\alpha$ -melanocyte-stimulating hormone; IBMX, 3-isobutyl-1-methylxanthine. \*\*\*  $p < 0.001$  and \*\*  $p < 0.01$  vs. stimulator-treated group; ###  $p < 0.001$  vs. untreated control.

### 2.8. In Situ B16F10 Cell Tyrosinase Inhibitory Activity of (Z)-BBTT Analogs 1 and 3

To identify the in situ cellular tyrosinase inhibitory activity of analogs **1** and **3**, B16F10 cells and L-DOPA were used as the experimental target cells and substrate for melanin synthesis, respectively. Kojic acid (10  $\mu$ M) was used for comparing the inhibitory activity. B16F10 cells were treated with test samples (**1**, **3**, and kojic acid) for 1 h, and then  $\alpha$ -MSH (1  $\mu$ M) and IBMX (200  $\mu$ M) were administered for 72 h to increase cellular tyrosinase activity. B16F10 cells were photographed after 2 h of treatment with excess L-DOPA, and the darkness of the cells was measured using the CS analyzer program (ATTO, Tokyo, Japan). Analogs **1** and **3** were used at 2, 5, and 10  $\mu$ M.

Treatment with  $\alpha$ -MSH and IBMX produced many cells with excessive melanin, whereas exposure to kojic acid significantly reduced the number of cells strongly stained with melanin (Figure 8). Analogs **1** and **3** reduced the number of strongly stained cells in a concentration-dependent manner. According to the results measuring relative dark areas of cells, the dark areas of **1** and **3** at 2  $\mu$ M were similar to that of kojic acid at 10  $\mu$ M, and when compared at the same concentration (10  $\mu$ M), the dark area of each analog (**1** and **3**) was significantly less than that of kojic acid. Thus, analogs **1** and **3** effectively inhibited tyrosinase activity in mammalian B16F10 cells.

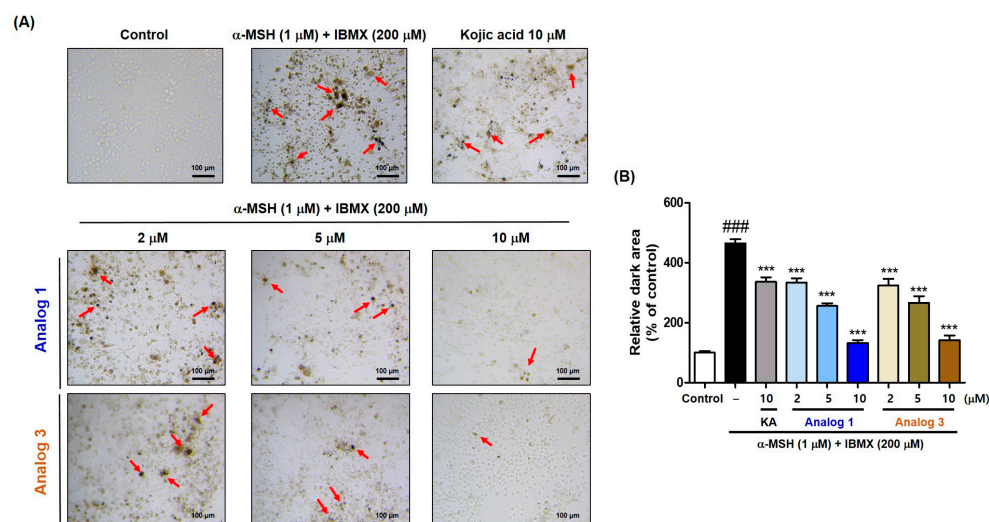


**Figure 8.** (A) In situ B16F10 cell tyrosinase activity determined using an L-DOPA staining method. Kojic acid (10 μM) was used as a positive reference standard. Test samples (kojic acid and analogs 1 and 3) were administered 1 h before treatment with α-MSH (1 μM) and IBMX (200 μM). The analogs were treated at 2, 5, and 10 μM. The results of in situ cellular tyrosinase activity were obtained 72 h after treatment with the analogs or kojic acid. Arrows indicate stained cells. Scale bar = 100 μm. (B) Relative amounts of stained areas were measured using an ATTO CS analyzer 3.2. α-MSH, α-melanocyte-stimulating hormone; IBMX, 3-isobutyl-1-methylxanthine; KA, kojic acid. ###  $p < 0.001$  vs. control; \*\*\*  $p < 0.001$  vs. α-MSH plus IBMX-treated group.

### 2.9. Antioxidant Capacity of (Z)-BBTT Analogs 1–12

As the antioxidant capacity of a compound is closely related to its anti-melanogenic effect [31], the ability of (Z)-BBTT analogs 1–12 to remove representative oxidant species such as ABTS<sup>+</sup> and DPPH radicals and ROS was investigated.

#### 2.9.1. ABTS<sup>+</sup> Radical-Scavenging Capacity

To measure the scavenging effects of analogs 1–12 on ABTS<sup>+</sup> radicals, ABTS was initially treated with potassium persulfate to yield ABTS<sup>•+</sup>. The formed ABTS<sup>+</sup> radical solution was mixed with test samples (analogs 1–12 and Trolox [positive reference standard]; final concentration: 100 μM), and absorbance was measured at 732 nm after storing for 2 min in the dark to determine %ABTS<sup>•+</sup>-scavenging ability.

Trolox exhibited strong ABTS<sup>•+</sup>-scavenging activity (99% scavenging), and five analogs (2–5 and 10) of 1–12 also showed strong ABTS<sup>•+</sup> inhibitory activity (>70%) (Figure 9A). In particular, analogs 2–4 showed very potent ABTS<sup>•+</sup> inhibitory efficacy with % scavenging activity ≥ 90%. Analogs 2 and 3 with catechol and resorcinol groups, respectively, had high potency with 99% and 98% ABTS<sup>•+</sup>-scavenging abilities, respectively, which were comparable to that of Trolox. Generally, analogs bearing a hydroxyl substituent on the β-phenyl ring showed potent ABTS<sup>•+</sup>-scavenging activity, whereas analogs without a hydroxyl substituent on the β-phenyl ring showed little ABTS<sup>•+</sup>-scavenging activity (2–5, 10, and 11 vs. 6–9).

#### 2.9.2. DPPH Radical-Scavenging Capacity

For measuring the scavenging effect of analogs 1–12 on DPPH radicals, test samples (analogs 1–12 and ascorbic acid [positive reference standard]; final concentration: 500 μM) were mixed with a DPPH solution, and absorbance was measured at 517 nm after storing for 30 min in the dark to determine % DPPH radical-scavenging ability.



Ascorbic acid and analog **2** bearing a catechol group showed strong radical-scavenging potential with 97 and 95% DPPH radical-scavenging abilities, respectively (Figure 9B). Analogs **3**, **4**, and **10**, which exerted potent ABTS<sup>•+</sup>-scavenging activity, also scavenged DPPH radicals by 41–58%. DPPH and ABTS<sup>•+</sup> radical-scavenging experiments showed similar trends; however, analog **5** showed a notable difference. Analog **5** demonstrated strong ABTS<sup>•+</sup> inhibitory activity with 71% ABTS<sup>•+</sup>-scavenging; however, it showed only 17% DPPH radical-scavenging activity, which was almost similar to that of analogs **6–9** without a hydroxyl substituent on the  $\beta$ -phenyl ring.

### 2.9.3. ROS-Scavenging Capacity

UV-A radiation induces ROS generation substantially, and oxidative stress accelerates melanin formation in organisms [32,33]. Thus, the ROS-scavenging ability of (*Z*)-BBTT analogs was examined to determine whether these analogs have an auxiliary ability to scavenge ROS. 3-Morpholinopyridone (SIN-1; 10  $\mu$ M) was used as a ROS generating substance, and Trolox (40  $\mu$ M) was used as a positive reference standard.

SIN-1 exposure significantly enhanced ROS levels, and treatment with Trolox significantly reduced the SIN-1-induced ROS levels (Figure 9C). All (*Z*)-BBTT analogs significantly reduced the SIN-1-induced ROS levels; however, most analogs weakly scavenged ROS except analogs **2** and **3** with 3,4-dihydroxy and 2,4-dihydroxy on the  $\beta$ -phenyl ring, respectively. Analog **3** showed ROS-scavenging activity equipotent to that of Trolox, whereas analog **2** exhibited greater ROS-scavenging potency than Trolox. The ROS-scavenging ability of these analogs may partially contribute to the inhibition of tyrosinase activity and melanogenesis.

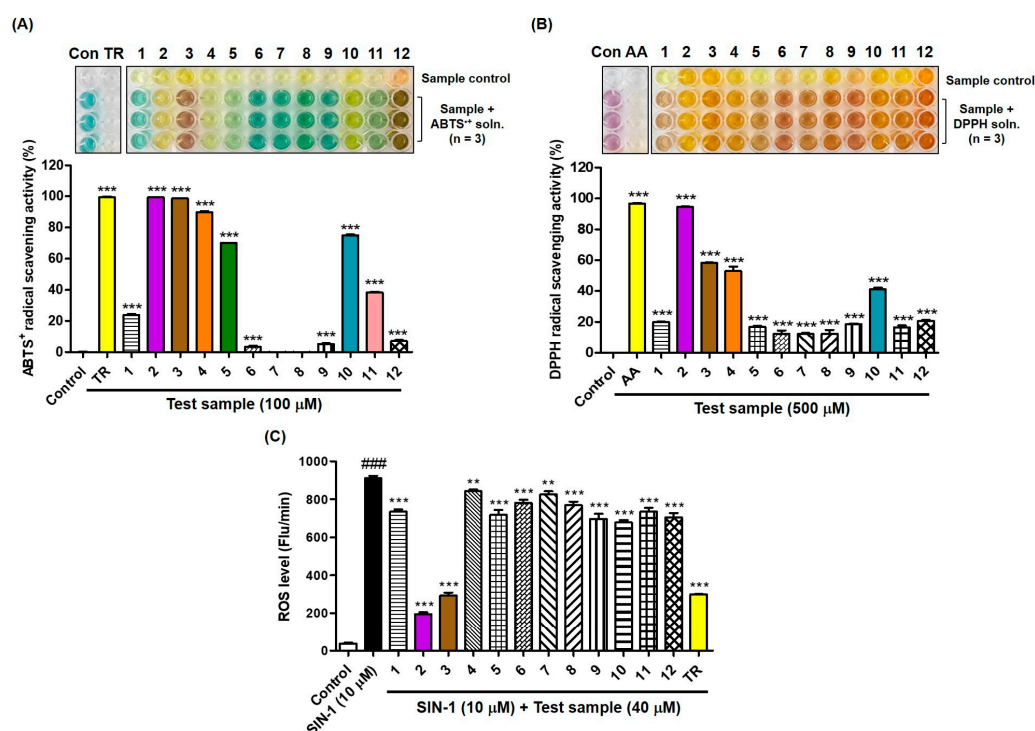


**Figure 9.** Antioxidant effects of (*Z*)-BBTT analogs **1–12** on radicals of ABTS<sup>•+</sup> (A) and DPPH (B) and ROS (C). (A) Analogs **1–12** and Trolox (TR; positive reference standard) were used at 100  $\mu$ M. (B) Analogs **1–12** and ascorbic acid (AA; positive reference standard) were used at 500  $\mu$ M. (C) Analogs **1–12**, Trolox (TR; positive reference standard), and SIN-1, a ROS generator, were used at 40, 40, and 10  $\mu$ M, respectively. In (A,B), \*\*\*  $p < 0.001$  vs. the control group and in (C), \*\*  $p < 0.01$  and \*\*\*  $p < 0.001$  vs. the SIN-1-treated group; ###  $p < 0.001$  vs. the control group. (*Z*)-BBTT, (*Z*)-3-benzyl-5-benzylidene-2-thioxothiazolidin-4-one; ABTS<sup>•+</sup>, 2,2'-azino-bis(3-ethylbenzothiazoline-6-sulfonic acid)

cation; DPPH, 2,2-diphenyl-1-picrylhydrazyl; SIN-1, 3-morpholinopyridone; ROS, reactive oxygen species.

### 2.10. Effects of Analogs 1–3 on HaCaT Cell Viability

As keratinocytes are one of the major cells that constitute the epidermis, the effects of analogs 1–3 on HaCaT (immortalized human keratinocytes) cell viability were investigated. Analogs 1–3 were tested at concentrations of 0, 2, 5, 10, and 20  $\mu\text{M}$ , and cell viability was determined 72 h after incubation.

None of the analogs showed significant cytotoxicity at any concentration tested (Figure 10). These results suggest that analogs 1 and 3 are promising candidates for skin-lightening agents, as they exhibit potent melanin production inhibition effects without perceptible cytotoxicity in the primary cells that constitute the epidermis.

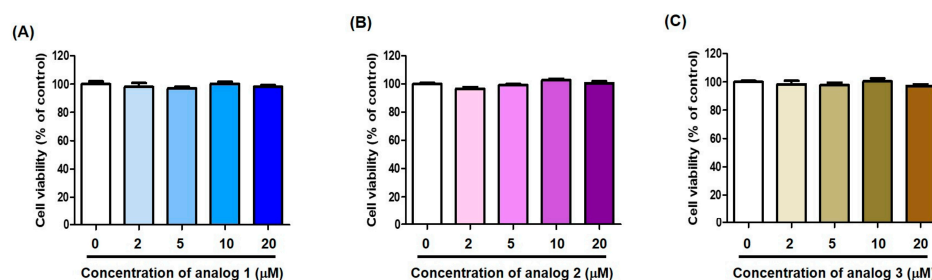


**Figure 10.** HaCaT cell viability in the presence of analogs 1–3 (A–C). All analogs were administered at concentrations of 0, 2, 5, 10, and 20  $\mu\text{M}$  for 72 h.

## 3. Materials and Methods

### 3.1. Synthesis

#### 3.1.1. General Methods

Thin-layer chromatography (TLC; Merck TLC Silica gel 60 F<sub>254</sub>, Darmstadt, Germany) was used to monitor the progress of the reactions. Chemical reagents were obtained from Daejung Chemicals (Siheung-si, Republic of Korea) and SEJIN CI Co., Ltd. (Seoul, Republic of Korea). All solvents were prepared in an anhydrous manner by distillation over Na/benzophenone or CaH<sub>2</sub>. Melting point of compounds were measured using a Stuart Scientific SMP3 Melting Point apparatus (Scientific Laboratory Supplies Ltd., Nottingham, UK). An expression compact mass spectrometer (Advion, Itasca, NY, USA) was utilized to obtain low-resolution mass (LR-MS) data, which were measured in the electrospray ionization negative or positive mode. High-resolution mass (HR-MS) data were acquired on a ZenoTOF 7600 mass spectrometer (SCIEX, Framingham, MA, USA). NMR data were obtained using a Varian Unity AS500 spectrometer (Agilent Technologies, Santa Clara, CA, USA) for 500 MHz <sup>1</sup>H-NMR and 125 MHz <sup>13</sup>C-NMR or a JEOL ECZ400S instrument (JEOL Ltd., Tokyo, Japan) for 400 MHz <sup>1</sup>H-NMR and 100 MHz <sup>13</sup>C-NMR. The chemical shifts ( $\delta$ ) and coupling constants (J) were recorded as ppm and Hz units, respectively. Peak splitting patterns were recorded as s (singlet), d (doublet), m (multiplet), brs (broad singlet), brd (broad doublet), or dd (doublet of doublets).

#### 3.1.2. Synthesis of 3-Benzyl-2-Thioxothiazolidin-4-One (13) [34,35]

Methyl thioglycolate (1.4 mL, 15.10 mmol) and triethylamine (2.1 mL, 15.07 mmol) were slowly added to a solution of benzyl isothiocyanate (2.0 mL, 15.08 mmol) in dichloromethane (DCM; 40 mL) at 0 °C. The reaction mixture was stirred at room temperature for 3.5 h. After the volatiles were evaporated in vacuo, a small amount of ether and appropriate amounts of hexane were added to the resulting residue to form solids. The generated



solids were filtered and washed with a mixture of ether and hexane (1:5) to afford pure 3-benzyl-2-thioxothiazolidin-4-one (**13**; 3.17 g, 94%).

$^1\text{H}$  NMR ( $\text{CDCl}_3$ , 400 MHz)  $\delta$  7.44–7.42 (dd, 2H,  $J$  = 7.6, 1.6 Hz, 2-H, 6-H), 7.33–7.28 (m, 3H, 3-H, 4-H, 5-H), 5.18 (s, 2H,  $\text{NCH}_2$ ), 3.97 (s, 2H,  $\text{SCH}_2$ );  $^{13}\text{C}$  NMR ( $\text{CDCl}_3$ , 100 MHz)  $\delta$  201.1, 174.0, 134.8, 129.1, 128.7, 128.3, 47.7, 35.5; molecular formula,  $\text{C}_{10}\text{H}_9\text{NOS}_2$ ; melting point, 80–81 °C; black-gray solid;  $R_f$  (hexane:ethyl acetate = 4:1 on silica gel TLC) = 0.42.

### 3.1.3. General Preparation of (Z)-BBTT Analogs 1–12

A solution of compound **13** (80 mg, 0.36 mmol) and an appropriate benzaldehyde (1.0 equiv.) in acetic acid (0.8 mL) was refluxed in sodium acetate (176 mg, 2.15 mmol) for 2–4 h. After cooling, cold water was added to the reaction mixtures. The generated solid was filtered and washed with water and, if necessary, additionally washed with DCM and hexane to furnish **1–12** in yields of 47–92%. All products were sufficiently pure for biological experiments.

- (Z)-3-Benzyl-5-(4-hydroxybenzylidene)-2-thioxothiazolidin-4-one (**1**).

$^1\text{H}$  NMR (dimethyl sulfoxide [ $\text{DMSO}$ ]- $d_6$ , 500 MHz)  $\delta$  10.51 (s, 1H, OH), 7.76 (s, 1H, vinyl H), 7.52 (d, 2H,  $J$  = 8.5 Hz, 2'-H, 6'-H), 7.35–7.26 (m, 5H, Ph), 6.94 (d, 2H,  $J$  = 8.5 Hz, 3'-H, 5'-H), 5.23 (s, 2H, benzyl  $\text{H}_2$ );  $^{13}\text{C}$  NMR ( $\text{DMSO}-d_6$ , 125 MHz)  $\delta$  193.7, 167.5, 161.2, 135.5, 134.7, 133.9, 129.0, 128.1 (2  $\times$  C), 124.4, 117.9, 117.1, 47.5; LR-MS (ESI $^-$ )  $m/z$  326 (M - H) $^-$ ; yield, 76%; molecular formula,  $\text{C}_{17}\text{H}_{13}\text{NO}_2\text{S}_2$ ; HR-MS (EDA)  $m/z$   $\text{C}_{17}\text{H}_{14}\text{NO}_2\text{S}_2$  (M + H) $^+$  calcd. 328.0466, obsd. 328.0460; melting point, 199–201 °C; brown solid;  $R_f$  (hexane:ethyl acetate = 3:1 on silica gel TLC) = 0.38.

- (Z)-3-Benzyl-5-(3,4-dihydroxybenzylidene)-2-thioxothiazolidin-4-one (**2**).

$^1\text{H}$  NMR ( $\text{DMSO}-d_6$ , 500 MHz)  $\delta$  10.06 (s, 1H, OH), 9.59 (s, 1H, OH), 7.68 (s, 1H, vinyl H), 7.35–7.25 (m, 5H, Ph), 7.08–7.04 (m, 2H, 2'-H, 6'-H), 6.90 (d, 1H,  $J$  = 8.5 Hz, 5'-H), 5.23 (s, 2H, benzyl  $\text{H}_2$ );  $^{13}\text{C}$  NMR ( $\text{DMSO}-d_6$ , 125 MHz)  $\delta$  193.7, 167.5, 150.1, 146.6, 135.5, 135.1 (2  $\times$  C), 129.0, 128.1, 125.9, 124.8, 117.7, 117.2, 117.0, 47.5; LR-MS (ESI $^-$ )  $m/z$  342 (M - H) $^-$ ; yield, 84%; molecular formula,  $\text{C}_{17}\text{H}_{13}\text{NO}_3\text{S}_2$ ; HR-MS (EDA)  $m/z$   $\text{C}_{17}\text{H}_{14}\text{NO}_3\text{S}_2$  (M + H) $^+$  calcd. 344.0415, obsd. 344.0410; melting point, 140–142 °C; brown solid;  $R_f$  (hexane:ethyl acetate = 3:1 on silica gel TLC) = 0.10.

- (Z)-3-Benzyl-5-(2,4-dihydroxybenzylidene)-2-thioxothiazolidin-4-one (**3**).

$^1\text{H}$  NMR ( $\text{DMSO}-d_6$ , 500 MHz)  $\delta$  10.76 (s, 1H, OH), 10.42 (s, 1H, OH), 7.99 (s, 1H, vinyl H), 7.35–7.25 (m, 5H, Ph), 7.22 (d, 1H,  $J$  = 8.5 Hz, 6'-H), 6.45–6.43 (m, 2H, 3'-H, 5'-H), 5.22 (s, 2H, benzyl  $\text{H}_2$ );  $^{13}\text{C}$  NMR ( $\text{DMSO}-d_6$ , 125 MHz)  $\delta$  193.9, 167.7, 163.3, 160.5, 135.6, 132.1, 130.4, 128.9, 128.0 (2  $\times$  C), 115.6, 112.4, 109.5, 102.9, 47.3; LR-MS (ESI $^-$ )  $m/z$  342 (M - H) $^-$ ; yield, 74%; molecular formula,  $\text{C}_{17}\text{H}_{13}\text{NO}_3\text{S}_2$ ; HR-MS (EDA)  $m/z$   $\text{C}_{17}\text{H}_{14}\text{NO}_3\text{S}_2$  (M + H) $^+$  calcd. 344.0415, obsd. 344.0412; melting point, 191–193 °C; copper-colored solid;  $R_f$  (hexane:ethyl acetate = 3:1 on silica gel TLC) = 0.10.

- (Z)-3-Benzyl-5-(4-hydroxy-3-methoxybenzylidene)-2-thioxothiazolidin-4-one (**4**).

$^1\text{H}$  NMR ( $\text{CDCl}_3$ , 500 MHz)  $\delta$  7.67 (s, 1H, vinyl H), 7.47 (d, 2H,  $J$  = 7.0 Hz, 2-H, 6-H), 7.33–7.28 (m, 3H, 3-H, 4-H, 5-H), 7.08 (brd, 1H,  $J$  = 8.0 Hz, 6'-H), 7.00 (d, 1H,  $J$  = 8.0 Hz, 5'-H), 6.95 (s, 1H, 2'-H), 6.04 (s, 1H, OH), 5.32 (s, 2H, benzyl  $\text{H}_2$ ), 3.95 (s, 3H,  $\text{OCH}_3$ );  $^{13}\text{C}$  NMR ( $\text{CDCl}_3$ , 125 MHz)  $\delta$  193.0, 167.9, 148.6, 147.1, 134.9, 133.9, 129.0, 128.6, 128.1, 126.4, 126.0, 119.8, 115.4, 112.0, 56.1, 47.5; LR-MS (ESI $^-$ )  $m/z$  356 (M - H) $^-$ ; yield, 68%; molecular formula,  $\text{C}_{18}\text{H}_{15}\text{NO}_3\text{S}_2$ ; melting point, 157–159 °C (lit. [19] 151–154 °C); brown solid;  $R_f$  (hexane:ethyl acetate = 3:1 on silica gel TLC) = 0.29.

- (Z)-3-Benzyl-5-(3-hydroxy-4-methoxybenzylidene)-2-thioxothiazolidin-4-one (5).  
 $^1\text{H}$  NMR ( $\text{CDCl}_3$ , 500 MHz)  $\delta$  7.64 (s, 1H, vinyl H), 7.47 (d, 2H,  $J = 7.0$  Hz, 2-H, 6-H), 7.33–7.27 (m, 3H, 3-H, 4-H, 5-H), 7.07–7.04 (m, 2H, 2'-H, 6'-H), 6.92 (d, 1H,  $J = 8.0$  Hz, 5'-H), 5.72 (s, 1H, OH), 5.32 (s, 2H, benzyl  $\text{H}_2$ ), 3.95 (s, 3H,  $\text{OCH}_3$ );  $^{13}\text{C}$  NMR ( $\text{CDCl}_3$ , 125 MHz)  $\delta$  193.3, 168.0, 148.9, 146.2, 134.9, 133.6, 129.0, 128.6, 128.1, 126.9, 124.6, 120.7, 116.1, 111.0, 56.2, 47.5; LR-MS (ESI<sup>-</sup>)  $m/z$  356 ( $\text{M} - \text{H}$ )<sup>-</sup>; yield, 54%; molecular formula,  $\text{C}_{18}\text{H}_{15}\text{NO}_3\text{S}_2$ ; melting point, 173–175 °C; yellow solid; Rf (hexane:ethyl acetate = 3:1 on silica gel TLC) = 0.28.
- (Z)-3-Benzyl-5-(4-methoxybenzylidene)-2-thioxothiazolidin-4-one (6).  
 $^1\text{H}$  NMR ( $\text{CDCl}_3$ , 500 MHz)  $\delta$  7.70 (s, 1H, vinyl H), 7.47 (d, 2H,  $J = 7.0$  Hz, 2-H, 6-H), 7.45 (d, 2H,  $J = 9.0$  Hz, 2'-H, 6'-H), 7.33–7.27 (m, 3H, 3-H, 4-H, 5-H), 6.99 (d, 2H,  $J = 9.0$  Hz, 3'-H, 5'-H), 5.32 (s, 2H, benzyl  $\text{H}_2$ ), 3.87 (s, 3H,  $\text{OCH}_3$ );  $^{13}\text{C}$  NMR ( $\text{CDCl}_3$ , 125 MHz)  $\delta$  193.2, 168.0, 161.8, 135.0, 133.5, 132.8, 129.0, 128.6, 128.1, 126.0, 119.9, 115.0, 55.6, 47.5; yield, 69%; molecular formula,  $\text{C}_{18}\text{H}_{15}\text{NO}_2\text{S}_2$ ; HR-MS (EDA)  $m/z$   $\text{C}_{18}\text{H}_{16}\text{NO}_2\text{S}_2$  ( $\text{M} + \text{H}$ )<sup>+</sup> calcd. 342.0622, obsd. 342.0619; melting point, 146–148 °C (lit. [19] 142–145 °C); copper-colored solid; Rf (hexane:ethyl acetate = 3:1 on silica gel TLC) = 0.63.
- (Z)-3-Benzyl-5-(3,4-dimethoxybenzylidene)-2-thioxothiazolidin-4-one (7).  
 $^1\text{H}$  NMR ( $\text{CDCl}_3$ , 500 MHz)  $\delta$  7.69 (s, 1H, vinyl H), 7.47 (d, 2H,  $J = 7.0$  Hz, 2-H, 6-H), 7.33–7.27 (m, 3H, 3-H, 4-H, 5-H), 7.13 (d, 1H,  $J = 8.5$  Hz, 6'-H), 6.97 (s, 1H, 2'-H), 6.95 (d, 1H,  $J = 8.5$  Hz, 5'-H), 5.32 (s, 2H, benzyl  $\text{H}_2$ ), 3.94 (s, 6H,  $2 \times \text{OCH}_3$ );  $^{13}\text{C}$  NMR ( $\text{CDCl}_3$ , 125 MHz)  $\delta$  193.0, 167.9, 151.6, 149.5, 134.9, 133.7, 129.0, 128.6, 128.1, 126.3, 125.7, 120.1, 112.4, 111.5, 56.1, 56.0, 47.5; LR-MS (ESI<sup>+</sup>)  $m/z$  372 ( $\text{M} + \text{H}$ )<sup>+</sup>, 394 ( $\text{M} + \text{Na}$ )<sup>+</sup>; yield, 52%; molecular formula,  $\text{C}_{19}\text{H}_{17}\text{NO}_3\text{S}_2$ ; melting point, 166–168 °C; yellow solid; Rf (hexane:ethyl acetate = 3:1 on silica gel TLC) = 0.45.
- (Z)-3-Benzyl-5-(2,4-dimethoxybenzylidene)-2-thioxothiazolidin-4-one (8).  
 $^1\text{H}$  NMR ( $\text{CDCl}_3$ , 500 MHz)  $\delta$  8.07 (s, 1H, vinyl H), 7.48 (d, 2H,  $J = 7.5$  Hz, 2-H, 6-H), 7.33–7.25 (m, 4H, 3-H, 4-H, 5-H, 6'-H), 6.57 (dd, 1H,  $J = 9.0, 2.0$  Hz, 5'-H), 6.45 (d, 1H,  $J = 2.0$  Hz, 3'-H), 5.32 (s, 2H, benzyl  $\text{H}_2$ ), 3.88 (s, 3H,  $\text{OCH}_3$ ), 3.86 (s, 3H,  $\text{OCH}_3$ );  $^{13}\text{C}$  NMR ( $\text{CDCl}_3$ , 125 MHz)  $\delta$  194.0, 168.1, 163.9, 160.4, 135.1, 132.1, 129.6, 129.0, 128.5, 128.0, 119.4, 115.7, 105.9, 98.5, 55.7, 55.6, 47.5; LR-MS (ESI<sup>+</sup>)  $m/z$  372 ( $\text{M} + \text{H}$ )<sup>+</sup>, 394 ( $\text{M} + \text{Na}$ )<sup>+</sup>; yield, 81%; molecular formula,  $\text{C}_{19}\text{H}_{17}\text{NO}_3\text{S}_2$ ; melting point, 156–158 °C; brown solid; Rf (hexane:ethyl acetate = 3:1 on silica gel TLC) = 0.76.
- (Z)-3-Benzyl-2-thioxo-5-(3,4,5-trimethoxybenzylidene)thiazolidin-4-one (9).  
 $^1\text{H}$  NMR ( $\text{CDCl}_3$ , 500 MHz)  $\delta$  7.65 (s, 1H, vinyl H), 7.46 (d, 2H,  $J = 7.0$  Hz, 2-H, 6-H), 7.33–7.25 (m, 3H, 3-H, 4-H, 5-H), 6.70 (s, 2H, 2'-H, 6'-H), 5.32 (s, 2H, benzyl  $\text{H}_2$ ), 3.92 (s, 3H,  $\text{OCH}_3$ ), 3.91 (s, 6H,  $2 \times \text{OCH}_3$ );  $^{13}\text{C}$  NMR ( $\text{CDCl}_3$ , 125 MHz)  $\delta$  192.9, 167.7, 153.7, 140.6, 134.8, 133.6, 129.0, 128.7, 128.6, 128.2, 121.8, 107.9, 61.1, 56.3, 47.6; LR-MS (ESI<sup>+</sup>)  $m/z$  402 ( $\text{M} + \text{H}$ )<sup>+</sup>, 424 ( $\text{M} + \text{Na}$ )<sup>+</sup>; yield, 78% molecular formula,  $\text{C}_{20}\text{H}_{19}\text{NO}_4\text{S}_2$ ; melting point, 108–110 °C; copper-colored solid; Rf (hexane:ethyl acetate = 3:1 on silica gel TLC) = 0.78.
- (Z)-3-Benzyl-5-(4-hydroxy-3,5-dimethoxybenzylidene)-2-thioxothiazolidin-4-one (10).  
 $^1\text{H}$  NMR ( $\text{CDCl}_3$ , 500 MHz)  $\delta$  7.63 (s, 1H, vinyl H), 7.46 (d, 2H,  $J = 7.0$  Hz, 2-H, 6-H), 7.33–7.25 (m, 3H, 3-H, 4-H, 5-H), 6.71 (s, 2H, 2'-H, 6'-H), 5.96 (s, 1H, OH), 5.31 (s, 2H, benzyl  $\text{H}_2$ ), 3.94 (s, 6H,  $2 \times \text{OCH}_3$ );  $^{13}\text{C}$  NMR ( $\text{CDCl}_3$ , 125 MHz)  $\delta$  192.9, 167.8, 147.5, 137.9, 134.9, 134.0, 128.9, 128.6, 128.1, 124.9, 120.1, 107.8, 56.5, 47.5; LR-MS (ESI<sup>+</sup>)  $m/z$  388 ( $\text{M} + \text{H}$ )<sup>+</sup>, 410 ( $\text{M} + \text{Na}$ )<sup>+</sup>; LR-MS (ESI<sup>-</sup>)  $m/z$  386 ( $\text{M} - \text{H}$ )<sup>-</sup>; yield, 92%; molecular formula,  $\text{C}_{19}\text{H}_{17}\text{NO}_4\text{S}_2$ ; melting point, 151–153 °C; copper-colored solid; Rf (hexane:ethyl acetate = 3:1 on silica gel TLC) = 0.68.

- (Z)-3-Benzyl-5-(3-bromo-4-hydroxybenzylidene)-2-thioxothiazolidin-4-one (**11**).  
 $^1\text{H}$  NMR ( $\text{CDCl}_3$ , 500 MHz)  $\delta$  7.62 (s, 1H, 2'-H), 7.60 (s, 1H, vinyl H), 7.46 (d, 2H,  $J = 7.0$  Hz, 2-H, 6-H), 7.37 (d, 1H,  $J = 8.5$  Hz, 6'-H), 7.33–7.27 (m, 3H, 3-H, 4-H, 5-H), 7.11 (d, 1H,  $J = 8.5$  Hz, 5'-H), 5.93 (brs, 1H, OH), 5.32 (s, 2H, benzyl H<sub>2</sub>);  $^{13}\text{C}$  NMR ( $\text{CDCl}_3$ , 125 MHz)  $\delta$  192.6, 167.8, 154.4, 134.8, 134.5, 131.9, 131.4, 129.0, 128.6, 128.2, 127.6, 121.8, 117.0, 111.4, 47.6; LR-MS (ESI<sup>-</sup>)  $m/z$  404 (M - H)<sup>-</sup>, 406 (M - H + 2)<sup>-</sup>; yield, 47%; molecular formula,  $\text{C}_{17}\text{H}_{12}\text{BrNO}_2\text{S}_2$ ; melting point, 154–156 °C; yellow solid; R<sub>f</sub> (hexane:ethyl acetate = 3:1 on silica gel TLC) = 0.34.
- (Z)-3-Benzyl-5-(3,5-dibromo-4-hydroxybenzylidene)-2-thioxothiazolidin-4-one (**12**).  
 $^1\text{H}$  NMR ( $\text{DMSO-d}_6$ , 500 MHz)  $\delta$  10.95 (brs, 1H, OH), 7.81 (s, 2H, 2'-H, 6'-H), 7.74 (s, 1H, vinyl H), 7.36–7.26 (m, 5H, Ph), 5.23 (s, 2H, benzyl H<sub>2</sub>);  $^{13}\text{C}$  NMR ( $\text{DMSO-d}_6$ , 125 MHz)  $\delta$  193.1, 167.2, 153.7, 135.3, 134.8, 131.3 (2 × C), 129.0, 128.1, 127.8, 121.8, 112.9, 47.6; LR-MS (ESI<sup>-</sup>)  $m/z$  482 (M - H)<sup>-</sup>, 484 (M - H + 2)<sup>-</sup>, 486 (M - H + 4)<sup>-</sup>; yield, 80%; molecular formula,  $\text{C}_{17}\text{H}_{11}\text{Br}_2\text{NO}_2\text{S}_2$ ; melting point, 179–181 °C; copper-colored solid; R<sub>f</sub> (hexane:ethyl acetate = 3:1 on silica gel TLC) = 0.26.

### 3.2. Mushroom Tyrosinase Inhibition Assay [36,37]

The inhibitory effects of the (Z)-BBTT analogs **1–12** on mushroom tyrosinase were examined in the presence of L-DOPA and L-tyrosine as substrates. Kojic acid and (Z)-BBTT analogs **4–12** were used at 2, 10, and 50  $\mu\text{M}$  regardless of substrates used; (Z)-BBTT analogs **1** and **2** were used at 0.4, 2, and 10  $\mu\text{M}$  in the presence of L-tyrosine and 2, 10, and 50  $\mu\text{M}$  in the presence of L-DOPA; and (Z)-BBTT analog **3** was used at 0.016, 0.08, and 0.4  $\mu\text{M}$  in the presence of L-tyrosine and 0.08, 0.4, and 2  $\mu\text{M}$  in the presence of L-DOPA to determine their IC<sub>50</sub> values. An aliquot (10  $\mu\text{L}$ ) of kojic acid or (Z)-BBTT analogs was mixed with mushroom tyrosinase aqueous solution (20  $\mu\text{L}$ ; 800 units/mL) and substrate mixture (170  $\mu\text{L}$ ) consisting of 17.2 mM sodium phosphate buffer (pH 6.5) and 345  $\mu\text{M}$  L-tyrosine or L-DOPA in each well of a 96-well plate. The plate was placed at 37 °C for 30 min, and well absorbance was measured at 475 nm to determine the generated dopachrome amounts in each well using a VersaMax<sup>®</sup> Elisa (VE) microplate reader (Molecular Devices, San Jose, CA, USA).

### 3.3. Kinetic Experiment in the Presence of (Z)-BBTT Analogs 1–3 and 6 Using Mushroom Tyrosinase [38–40]

Kinetic experiments were performed by measuring the initial dopachrome generation rate of mushroom tyrosinase. An aliquot (10  $\mu\text{L}$ ) of (Z)-BBTT analogs **1–3** and **6** was mixed with mushroom tyrosinase aqueous solution (20  $\mu\text{L}$ ; 150 units/mL) and substrate mixture (170  $\mu\text{L}$ ) consisting of 17.2 mM sodium phosphate buffer (pH 6.5) and L-DOPA aqueous solution of various concentrations (1, 2, 4, 8, and 16 mM) in each well of a 96-well plate. During the 30 min incubation, well absorbance was recorded at 475 nm every 5 min using a VE microplate reader. Analogs **1–3** and **6** were used at the following concentrations: 0, 20, 40, and 80  $\mu\text{M}$  for **1**; 0, 15, 30, and 60  $\mu\text{M}$  for **2**; 0, 0.1, 0.2, and 0.4  $\mu\text{M}$  for **3**; and 0, 12.5, 25, and 50  $\mu\text{M}$  for **6**. The Lineweaver–Burk plot for each analog was obtained by plotting the reciprocal of the initial dopachrome formation rate versus the reciprocal of the substrate concentration.

### 3.4. Docking Simulation of Mushroom Tyrosinase and (Z)-BBTT Analogs 1–3 and 6 [41,42]

For the in silico docking simulation between mushroom tyrosinase and the (Z)-BBTT analogs **1–3** and **6**, the three-dimensional (3D) X-ray structure of the mushroom tyrosinase protein was acquired from the Protein Data Bank: 2Y9X (*Agaricus bisporus*)

(<http://www.rcsb.org>, accessed on 1 September 2024). The cocrystal structure of 2Y9X contains tropolone as the ligand at the active site. Kojic acid was used as a positive reference standard. The 3D structures of the ligands (kojic acid and analogs 1–3 and 6) were acquired through energy minimization using Chem3D Pro 12.0. After removing tropolone bound to the tyrosinase active site, the 3D structure of tyrosinase was docked with the ligand 3D structures using AutoDock Vina (ver. 1.2.0). The binding energies between the ligands and tyrosinase were determined using AutoDock Vina and Chimera 1.17.3 (<https://www.cgl.ucsf.edu/chimera/download.html>, accessed on 15 October 2024). LigandScout 4.4.8 (<http://www.inteligand.com/ligandscout/download.shtml>, accessed on 20 October 2024) provided the plausible chemical interactions between the ligands and tyrosinase.

### 3.5. Cell Culture [42,43]

Murine B16F10 and human keratinocyte HaCaT cells were cultivated in a solution consisting of Dulbecco's modified Eagle's medium (Welgene, Gyeongsan-si, Republic of Korea), 10% heat-inactivated fetal bovine serum (Gibco, Grand Island, NY, USA), and 1% penicillin–streptomycin solution (100×) at 37 °C in a humidified environment with 5% CO<sub>2</sub>.

### 3.6. Cytotoxicity Assay on B16F10 Murine Melanoma Cells [44]

The influence of (Z)-BBTT analogs 1–3 on B16F10 cell viability was studied using an EZ-Cytox solution (EZ-1000®, DoGenBio, Seoul, Republic of Korea). B16F10 cells were seeded at a density of  $1 \times 10^3$  in each well of a 96-well plate, and the plate was cultivated under normal cell culture conditions for 24 h. Analogs were added to each well at concentrations of 0, 1, 2, 5, and 10 µM, and then cells were cultivated for 72 h under normal cell culture conditions. An aliquot (10 µL) of the EZ-Cytox solution was added to each well and cultivated for 2 h. Well absorbance was recorded at 450 nm using a VE microplate reader to calculate cell viability.

### 3.7. Cellular Melanin Level Measurement in the Presence of (Z)-BBTT Analogs 1 and 3 in B16F10 Cells [44]

B16F10 cells were seeded at a density of 5000 per well of a 6-well plate, and the plate was cultivated under normal cell culture conditions for 24 h. Kojic acid was utilized for comparing activities. Analog (1 and 3) or kojic acid was added to each well at concentrations of 0, 2, 5, and 10 µM and 10 µM, respectively, and then cultivated for 1 h under normal cell culture conditions. In addition, 200 µM IBMX and 1 µM α-MSH (Alomone Labs™, Jerusalem, Israel) were added to each well and cultivated for 72 h under the normal cell culture conditions. To determine the cellular melanin levels, 1N–NaOH solution (100 µL) was added to each well and then kept at 60 °C for 1 h to lyse the cells. The cell lysates were washed twice with phosphate-buffered saline (PBS) and transferred to a 96-well plate, and the absorbance was recorded at 405 nm using a VE microplate reader to determine the cellular melanin content.

### 3.8. Cellular Tyrosinase Activity Measurement in the Presence of (Z)-BBTT Analogs 1 and 3 in B16F10 Cells [44]

B16F10 cells were seeded at a density of 5000 per well of a 6-well plate, and the plate was cultivated under normal cell culture conditions for 24 h. Kojic acid was utilized for comparing activities. Analog (1 and 3) or kojic acid was added to each well at concentrations of 0, 2, 5, and 10 µM and 10 µM, respectively, and then cultivated for 1 h under normal cell culture conditions. Stimulators (200 µM IBMX and 1 µM α-MSH) were added to each well and cultivated for 72 h under normal cell culture conditions. To determine

cellular tyrosinase activity, the cells were washed twice with PBS, treated with lysis buffer solution (100  $\mu$ L) comprising 50 mM phosphate buffer (pH 6.5) (90  $\mu$ L), 2 mM phenylmethanesulfonyl fluoride (5  $\mu$ L), and 20% Triton X-100 (5  $\mu$ L), and incubated at  $-80$   $^{\circ}$ C for 30 min. After centrifugation (10,000 $\times$  g, 4  $^{\circ}$ C, and 10 min), the supernatants (80  $\mu$ L each) were transferred to each well of a 96-well plate, then 10 mM L-DOPA (20  $\mu$ L) was added to each well. The absorbance was measured at 475 nm at 1 min intervals for 10 min using a VE microplate reader to determine cellular tyrosinase activity.

### 3.9. Measurement of In Situ Cellular Tyrosinase Activity in B16F10 Cells [44,45]

To evaluate in situ cellular tyrosinase activity, test samples (kojic acid [positive reference standard] and analogs **1** and **3**) were added to each well of a 24-well plate containing B16F10 cells incubated for 24 h at a density of  $1 \times 10^3$  cells/well. Kojic acid and the two analogs were used at final concentrations of 10 and 2, 5, and 10  $\mu$ M, respectively. After 1 h, the cells were exposed to 1  $\mu$ M  $\alpha$ -MSH and 200  $\mu$ M IBMX and cultivated under normal cell culture conditions for 72 h. Cultured cells were fixed using a 4% paraformaldehyde solution for 40 min, washed twice with PBS, and permeabilized using 0.1% Triton X-100 for 2 min. L-DOPA solution (2 mM; 500  $\mu$ L) was added to each well after washing twice with PBS. After the plate was placed for 2 h at 37  $^{\circ}$ C, the images for cell staining were acquired using a camera attached to a microscope (Motic, Hong Kong).

### 3.10. ABTS<sup>••</sup> Scavenging Activity [46,47]

ABTS<sup>••</sup> was prepared by mixing equal amounts of ABTS (14 mM in H<sub>2</sub>O) and K<sub>2</sub>S<sub>2</sub>O<sub>8</sub> (4.9 mM in H<sub>2</sub>O) and storing in the dark at 20  $^{\circ}$ C for 16 h. Prior to use, the absorbance of the prepared ABTS<sup>••</sup> solution was adjusted to  $0.7 \pm 0.02$  at 732 nm by dilution with methanol. A cosolvent (EtOH:DMSO = 10:1 [*v/v*]) was used to prepare solutions of the test samples (analog **1–12** and Trolox [positive reference standard]). All test samples were used at a final concentration of 100  $\mu$ M. The test sample solution (10  $\mu$ L) was mixed with the adjusted ABTS<sup>••</sup> solution (90  $\mu$ L) in each well of a 96-well plate, and the mixture was kept in the dark at 20  $^{\circ}$ C for 2 min. The absorbance was recorded at 732 nm at 1 min intervals for 10 min using a VE microplate reader. The percentage of radical-scavenging activity was calculated using the formula % radical-scavenging activity =  $[(\text{Abs}_{\text{control}} - \text{Abs}_{\text{sample}})/\text{Abs}_{\text{control}}] \times 100$ , where  $\text{Abs}_{\text{sample}}$  and  $\text{Abs}_{\text{control}}$  are absorbances of the sample and control, respectively.

### 3.11. DPPH Radical-Scavenging Activity [48,49]

L-Ascorbic acid was used as a positive control. Test samples (analog **1–12** and L-ascorbic acid; 5 mM, 20  $\mu$ L) dissolved in DMSO were added to each well of a 96-well plate containing the DPPH methanol solution (0.2 mM, 180  $\mu$ L), and the plate was placed in the dark at 20  $^{\circ}$ C for 30 min. The absorbance was recorded at 517 nm using a VE microplate reader to calculate DPPH radical-scavenging activity.

### 3.12. ROS-Scavenging Activity [50,51]

The test samples ((*Z*)-BBTT analog **1–12** and Trolox [positive reference standard]) and 3-morpholinopyridone (SIN-1) were dissolved in DMSO and PBS, respectively. To prepare 2',7'-dichlorodihydrofluorescein (DCFH) solution, PBS (50 mM; 4.9 mL, pH 7.4) and DCFH diacetate (2.5 mM; 0.05 mL) were mixed with esterase (15 units/10 mL; 0.05 mL). After storage for 30 min at 20  $^{\circ}$ C, the mixture was placed in the dark until further use. SIN-1 (10  $\mu$ L) was added to each well of a 96-well black plate containing PBS (180  $\mu$ L) and test sample (10  $\mu$ L), and the plate was placed in the dark for 5 min. The prepared DCFH solution (50  $\mu$ L) was added to each well of the black plate. The fluorescence of each well was recorded at 535 nm using a microplate reader (Berthold Advances GmbH & Co.,

Bad Wildbad, Germany) at an excitation wavelength of 485 nm. The test samples and SIN-1 were tested at final concentrations of 40 and 10  $\mu$ M, respectively.

### 3.13. Cytotoxicity Assay on HaCaT Cells [42]

The effect of (*Z*)-BBTT analogs 1–3 on HaCaT cell viability was examined using EZ-Cytox solution. HaCaT cells were seeded at a density of  $1 \times 10^3$  in each well of a 96-well plate, and the plate was cultivated under normal cell culture conditions for 24 h. Analogs 1–3 were added to each well at concentrations of 0, 2, 5, 10, and 20  $\mu$ M and then cultivated for 72 h under normal cell culture conditions. An aliquot (10  $\mu$ L) of the EZ-Cytox solution was added to each well and cultivated for 2 h. Well absorbance was recorded at 450 nm using a VE microplate reader to calculate HaCaT cell viability.

### 3.14. Statistical Analysis

All assays were performed independently at least three times to determine statistical significance. The results are described as means  $\pm$  standard errors of the mean (SEM). Significance was determined using GraphPad Prism 5 (La Jolla, CA, USA) via a one-way analysis of variance (ANOVA) followed by the Newman–Keuls test. Significance was set at  $p < 0.05$ .

## 4. Conclusions

(*Z*)-BBTT analogs 1–12 were designed and synthesized as novel tyrosinase inhibitors based on the structures of a  $\beta$ -phenyl- $\alpha,\beta$ -unsaturated carbonyl motif and a 3-benzyl-2-thioxothiazolidin-4-one scaffold. Analogs 1–3 exhibited strong inhibitory activity against mushroom tyrosinase. In particular, the  $IC_{50}$  value of analog 3 was found to be in the range of tens of nanomoles. Kinetic studies demonstrated analogs 1–3 and 6 to be competitive inhibitors, and *in silico* studies supported the results. Experiments using B16F10 mammalian cells demonstrated that analogs 1 and 3 strongly inhibited melanin production through their anti-tyrosinase activities. Furthermore, analogs 1 and 3 showed no perceptible cytotoxicity in HaCaT and B16F10 cells, and analog 3 exhibited strong antioxidant efficacy in various antioxidant experiments.

**Supplementary Materials:** The following supporting information can be downloaded at: <https://www.mdpi.com/article/10.3390/molecules30030517/s1>.

**Author Contributions:** Conceptualization, P.C. and H.R.M.; formal analysis, H.S.P. (Hyeon Seo Park), H.J.J., H.S.P. (Hye Soo Park) and H.J.K.; funding acquisition, H.R.M.; resources, H.S.P. (Hyeon Seo Park), H.S.P. (Hye Soo Park), and H.J.K.; software, H.S.P. (Hyeon Seo Park) and P.C.; supervision, H.Y.C. and H.R.M.; validation, Y.P., H.J.J. and H.J.K.; writing—original draft, H.J.J. and H.R.M.; writing—review and editing, P.C., H.Y.C. and H.R.M. All authors have read and agreed to the published version of the manuscript.

**Funding:** This study was supported by a National Research Foundation of Korea (NRF) grant funded by the Korean government (MIST) (Grant No. NRF-2020R1A2C1004198) and the Basic Science Research Program through the National Research Foundation (NRF) of Korea funded by the Ministry of Education (Grant no. NRF-2021R111A1A01052284).

**Institutional Review Board Statement:** Not applicable.

**Informed Consent Statement:** Not applicable.

**Data Availability Statement:** The data presented in this study are available in the article and Supplementary Materials.

**Conflicts of Interest:** The authors declare no conflicts of interest.



## References

1. Rai, R.; Shanmuga, S.C.; Srinivas, C. Update on photoprotection. *Indian J. Dermatol.* **2012**, *57*, 335–342. <https://doi.org/10.4103/0019-5154.100472>.
2. Holick, M.F. Sunlight and vitamin D for bone health and prevention of autoimmune diseases, cancers, and cardiovascular disease. *Am. J. Clin. Nutr.* **2004**, *80*, 1678s–1688s. <https://doi.org/10.1093/ajcn/80.6.1678S>.
3. Holick, M.F. Sunlight, ultraviolet radiation, vitamin D and skin cancer: How much sunlight do we need? *Adv. Exp. Med. Biol.* **2014**, *810*, 1–16.
4. Kaidbey, K.H.; Agin, P.P.; Sayre, R.M.; Kligman, A.M. Photoprotection by melanin—A comparison of black and Caucasian skin. *J. Am. Acad. Dermatol.* **1979**, *1*, 249–260. [https://doi.org/10.1016/s0190-9622\(79\)70018-1](https://doi.org/10.1016/s0190-9622(79)70018-1).
5. Meredith, P.; Sarna, T. The physical and chemical properties of eumelanin. *Pigment. Cell Res.* **2006**, *19*, 572–594.
6. Lin, J.Y.; Fisher, D.E. Melanocyte biology and skin pigmentation. *Nature* **2007**, *445*, 843–850. <https://doi.org/10.1038/nature05660>.
7. Gray-Schopfer, V.; Wellbrock, C.; Marais, R. Melanoma biology and new targeted therapy. *Nature* **2007**, *445*, 851–857.
8. Rittié, L.; Fisher, G.J. Natural and sun-induced aging of human skin. *Cold Spring Harb. Perspect. Med.* **2015**, *5*, a015370.
9. Wasmeier, C.; Hume, A.N.; Bolasco, G.; Seabra, M.C. Melanosomes at a glance. *J. Cell Sci.* **2008**, *121*, 3995–3999. <https://doi.org/10.1242/jcs.040667>.
10. Ito, S.; Wakamatsu, K. Human hair melanins: What we have learned and have not learned from mouse coat color pigmentation. *Pigment. Cell Melanoma Res.* **2011**, *24*, 63–74.
11. Ito, S.; Wakamatsu, K. Chemistry of mixed melanogenesis—Pivotal roles of dopaquinone. *Photochem. Photobiol.* **2008**, *84*, 582–592.
12. Hearing, V.J.; Tsukamoto, K. Enzymatic control of pigmentation in mammals. *FASEB J.* **1991**, *5*, 2902–2909.
13. Ito, S. A Chemist's View of Melanogenesis. *Pigment. Cell Res.* **2003**, *16*, 230–236. <https://doi.org/10.1034/j.1600-0749.2003.00037.x>.
14. Decker, H.; Schweikardt, T.; Tuczec, F. The first crystal structure of tyrosinase: All questions answered? *Angew. Chem. Int. Ed. Engl.* **2006**, *45*, 4546–4550. <https://doi.org/10.1002/anie.200601255>.
15. Lai, X.; Wichers, H.J.; Soler-Lopez, M.; Dijkstra, B.W. Structure and Function of Human Tyrosinase and Tyrosinase-Related Proteins. *Chem.—A Eur. J.* **2018**, *24*, 47–55. <https://doi.org/10.1002/chem.201704410>.
16. Pillaiyar, T.; Manickam, M.; Namasivayam, V. Skin whitening agents: Medicinal chemistry perspective of tyrosinase inhibitors. *J. Enzym. Inhib. Med. Chem.* **2017**, *32*, 403–425. <https://doi.org/10.1080/14756366.2016.1256882>.
17. Rodríguez-López, J.; Serna-Rodríguez, P.; Tudela, J.; Varón, R.; García-Cánovas, F. A continuous spectrophotometric method for the determination of diphenolase activity of tyrosinase using 3, 4-dihydroxymandelic acid. *Anal. Biochem.* **1991**, *195*, 369–374.
18. Gentili, V.; Turrin, G.; Marchetti, P.; Rizzo, S.; Schiuma, G.; Beltrami, S.; Cristofori, V.; Illuminati, D.; Compagnin, G.; Trapella, C.; et al. Synthesis and biological evaluation of novel rhodanine-based structures with antiviral activity towards HHV-6 virus. *Bioorganic Chem.* **2022**, *119*, 105518. <https://doi.org/10.1016/j.bioorg.2021.105518>.
19. Mandal, S.P.; Garg, A.; Sahetya, S.S.; Nagendra, S.R.; Sripad, H.S.; Manjunath, M.M.; Soni, M.; Baig, R.N.; Kumar, S.V.; Kumar, B.P. Novel rhodanines with anticancer activity: Design, synthesis and CoMSIA study. *RSC Adv.* **2016**, *6*, 58641–58653. <https://doi.org/10.1039/C6RA08785J>.
20. Han, L.; Zhao, L.; Wang, H.; Dou, T.; Guo, F.; Qi, J.; Xu, W.; Piao, L.; Jin, X.; Fen'er, C.; et al. Synthesis, Antibacterial and Antifungal Evaluation of Rhodanine Derivatives Bearing Quinoxaliny Imidazole Moiety as ALK5 Inhibitors. *Chin. J. Org. Chem.* **2021**, *41*, 4428–4436.
21. Martinez, A.; Alonso, M.; Castro, A.; Dorronsoro, I.; Gelpí, J.L.; Luque, F.J.; Pérez, C.; Moreno, F.J. SAR and 3D-QSAR studies on thiazolidinone derivatives: Exploration of structural requirements for glycogen synthase kinase 3 inhibitors. *J. Med. Chem.* **2005**, *48*, 7103–7112. <https://doi.org/10.1021/jm040895g>.
22. Dastyafteh, N.; Noori, M.; Montazer, M.N.; Zomorodian, K.; Yazdanpanah, S.; Iraj, A.; Ghomi, M.K.; Javanshir, S.; Asadi, M.; Dianatpour, M.; et al. New thioxothiazolidinyl-acetamides derivatives as potent urease inhibitors: Design, synthesis, in vitro inhibition, and molecular dynamic simulation. *Sci. Rep.* **2023**, *13*, 21. <https://doi.org/10.1038/s41598-022-27234-3>.
23. Griffett, K. Targeting Nuclear Receptors for Chronic Inflammatory Pain: A Potential Alternative. *ACS Pharmacol. Transl. Sci.* **2022**, *5*, 440–444. <https://doi.org/10.1021/acspsci.2c00063>.
24. Cheng, S.; Zou, Y.; Chen, X.; Chen, J.; Wang, B.; Tian, J.; Ye, F.; Lu, Y.; Huang, H.; Lu, Y.; et al. Design, synthesis and biological evaluation of 3-substituted-2-thioxothiazolidin-4-one (rhodanine) derivatives as antitubercular agents against *Mycobacterium tuberculosis* protein tyrosine phosphatase B. *Eur. J. Med. Chem.* **2023**, *58*, 115571. <https://doi.org/10.1016/j.ejmech.2023.115571>.

25. Ullah, S.; Kang, D.; Lee, S.; Ikram, M.; Park, C.; Park, Y.; Yoon, S.; Chun, P.; Moon, H.R. Synthesis of cinnamic amide derivatives and their anti-melanogenic effect in  $\alpha$ -MSH-stimulated B16F10 melanoma cells. *Eur. J. Med. Chem.* **2019**, *161*, 78–92. <https://doi.org/10.1016/j.ejmech.2018.10.025>.
26. Choi, H.; Ryu, I.Y.; Choi, I.; Ullah, S.; Jung, H.J.; Park, Y.; Hwang, Y.; Jeong, Y.; Hong, S.; Chun, P.; et al. Identification of (Z)-2-benzylidene-dihydroimidazo[thiazolone] derivatives as tyrosinase inhibitors: Anti-melanogenic effects and in silico studies. *Comput. Struct. Biotechnol. J.* **2022**, *20*, 899–912. <https://doi.org/10.1016/j.csbj.2022.02.007>.
27. Lee, J.; Jeong, Y.; Jung, H.J.; Ullah, S.; Ko, J.; Kim, G.Y.; Yoon, D.; Hong, S.; Kang, D.; Park, Y.; et al. Anti-tyrosinase flavone derivatives and their anti-melanogenic activities: Importance of the  $\beta$ -phenyl- $\alpha,\beta$ -unsaturated carbonyl scaffold. *Bioorganic Chem.* **2023**, *135*, 106504. <https://doi.org/10.1016/j.bioorg.2023.106504>.
28. Yoon, D.; Kang, M.K.; Jung, H.J.; Ullah, S.; Lee, J.; Jeong, Y.; Noh, S.G.; Kang, D.; Park, Y.; Chun, P.; et al. Design, Synthesis, In Vitro, and In Silico Insights of 5-(Substituted benzylidene)-2-phenylthiazol-4(5H)-one Derivatives: A Novel Class of Anti-Melanogenic Compounds. *Molecules* **2023**, *28*, 3293.
29. Park, Y.J.; Jung, H.J.; Kim, H.J.; Park, H.S.; Lee, J.; Yoon, D.; Kang, M.K.; Kim, G.Y.; Ullah, S.; Kang, D.; et al. Thiazol-4(5H)-one analogs as potent tyrosinase inhibitors: Synthesis, tyrosinase inhibition, antimelanogenic effect, antioxidant activity, and in silico docking simulation. *Bioorganic Med. Chem.* **2024**, *98*, 117578. <https://doi.org/10.1016/j.bmc.2023.117578>.
30. Vögeli, U.; von Philipsborn, W.; Nagarajan, K.; Nair, M.D. Structures of Addition Products of Acetylenedicarboxylic Acid Esters with Various Dinucleophiles. An application of C, H-spin-coupling constants. *Helv. Chim. Acta* **1978**, *61*, 607–617. <https://doi.org/10.1002/hlca.19780610207>.
31. Searle, T.; Al-Niaimi, F.; Ali, F.R. The top 10 cosmeceuticals for facial hyperpigmentation. *Dermatol. Ther.* **2020**, *33*, e14095. <https://doi.org/10.1111/dth.14095>.
32. Chaiprasongsuk, A.; Onkoksoong, T.; Pluemsamran, T.; Limsaengurai, S.; Panich, U. Photoprotection by dietary phenolics against melanogenesis induced by UVA through Nrf2-dependent antioxidant responses. *Redox Biol.* **2016**, *8*, 79–90. <https://doi.org/10.1016/j.redox.2015.12.006>.
33. Fu, W.; Wu, Z.; Zheng, R.; Yin, N.; Han, F.; Zhao, Z.; Dai, M.; Han, D.; Wang, W.; Niu, L. Inhibition mechanism of melanin formation based on antioxidant scavenging of reactive oxygen species. *Analyst* **2022**, *147*, 2703–2711. <https://doi.org/10.1039/D2AN00588C>.
34. Roosta, A.; Alizadeh, A.; Rezaieyehraad, R.; Khanpour, M. Efficient and Chemoselective Procedure for Conversion of Rhodanine Derivatives into 1,3-Thiazolidine-2,4-diones via 1,3-Dipolar Cycloaddition Reaction and Rearrangement Sequences. *ChemistrySelect* **2020**, *5*, 12531–12534. <https://doi.org/10.1002/slct.202003484>.
35. Alizadeh, A.; Chelebari, E.A.; Rezaieyehraad, R. Regio- and Chemoselective Synthesis of 4,6-Dithia-1,2,9-triazaspiro [4.4]non-2-en-8-ones through an Ultrasound-Promoted One-Pot Sequential Pseudo-Five-Component Reaction. *Synthesis* **2024**, *56*, 3199–3205. <https://doi.org/10.1055/s-0043-1775386>.
36. Hyun, S.K.; Lee, W.-H.; Jeong, D.M.; Kim, Y.; Choi, J.S. Inhibitory Effects of Kurarinol, Kuraridinol, and Trifolirhizin from *Sophora flavescens* on Tyrosinase and Melanin Synthesis. *Biol. Pharm. Bull.* **2008**, *31*, 154–158. <https://doi.org/10.1248/bpb.31.154>.
37. Bang, E.; Noh, S.G.; Ha, S.; Jung, H.J.; Kim, D.H.; Lee, A.K.; Hyun, M.K.; Kang, D.; Lee, S.; Park, C.; et al. Evaluation of the Novel Synthetic Tyrosinase Inhibitor (Z)-3-(3-bromo-4-hydroxybenzylidene)thiochroman-4-one (MHY1498) In Vitro and In Silico. *Molecules* **2018**, *23*, 3307. <https://doi.org/10.3390/molecules23123307>.
38. Lineweaver, H.; Burk, D. The Determination of Enzyme Dissociation Constants. *J. Am. Chem. Soc.* **1934**, *56*, 658–666. <https://doi.org/10.1021/ja01318a036>.
39. Dixon, M. The determination of enzyme inhibitor constants. *Biochem. J.* **1953**, *55*, 170–171. <https://doi.org/10.1042/bj0550170>.
40. Jung, H.J.; Kim, H.J.; Park, H.S.; Kim, G.Y.; Park, Y.J.; Lee, J.; Kang, M.K.; Yoon, D.; Kang, D.; Park, Y.; et al. Highly potent anti-melanogenic effect of 2-thiobenzothiazole derivatives through nanomolar tyrosinase activity inhibition. *Bioorganic Chem.* **2024**, *150*, 107586. <https://doi.org/10.1016/j.bioorg.2024.107586>.
41. Kim, H.J.; Jung, H.J.; Kim, Y.E.; Jeong, D.; Park, H.S.; Park, H.S.; Kang, D.; Park, Y.; Chun, P.; Chung, H.Y.; et al. Investigation of the Efficacy of Benzylidene-3-methyl-2-thioxothiazolidin-4-one Analogs with Antioxidant Activities on the Inhibition of Mushroom and Mammal Tyrosinases. *Molecules* **2024**, *29*, 2887.
42. Jung, H.J.; Park, H.S.; Park, H.S.; Kim, H.J.; Yoon, D.; Park, Y.; Chun, P.; Chung, H.Y.; Moon, H.R. Exploration of Compounds with 2-Phenylbenzo[d]oxazole Scaffold as Potential Skin-Lightening Agents through Inhibition of Melanin Biosynthesis and Tyrosinase Activity. *Molecules* **2024**, *29*, 4162.
43. Oh, T.I.; Yun, J.M.; Park, E.J.; Kim, Y.S.; Lee, Y.M.; Lim, J.H. Plumbagin Suppresses  $\alpha$ -MSH-Induced Melanogenesis in B16F10 Mouse Melanoma Cells by Inhibiting Tyrosinase Activity. *Int. J. Mol. Sci.* **2017**, *18*, 320. <https://doi.org/10.3390/ijms18020320>.

44. Moon, K.M.; Yang, J.H.; Lee, M.K.; Kwon, E.B.; Baek, J.; Hwang, T.; Kim, J.I.; Lee, B. Maclurin Exhibits Antioxidant and Anti-Tyrosinase Activities, Suppressing Melanogenesis. *Antioxidants* **2022**, *11*, 1164. <https://doi.org/10.3390/antiox11061164>.
45. Moon, S.Y.; Akter, K.M.; Ahn, M.J.; Kim, K.D.; Yoo, J.; Lee, J.H.; Lee, J.H.; Hwangbo, C. Fraxinol Stimulates Melanogenesis in B16F10 Mouse Melanoma Cells through CREB/MITF Signaling. *Molecules* **2022**, *27*, 1549. <https://doi.org/10.3390/molecules27051549>.
46. Re, R.; Pellegrini, N.; Proteggente, A.; Pannala, A.; Yang, M.; Rice-Evans, C. Antioxidant activity applying an improved ABTS radical cation decolorization assay. *Free. Radic. Biol. Med.* **1999**, *26*, 1231–1237. [https://doi.org/10.1016/S0891-5849\(98\)00315-3](https://doi.org/10.1016/S0891-5849(98)00315-3).
47. Nenadis, N.; Wang, L.-F.; Tsimidou, M.; Zhang, H.-Y. Estimation of Scavenging Activity of Phenolic Compounds Using the ABTS<sup>+</sup> Assay. *J. Agric. Food Chem.* **2004**, *52*, 4669–4674. <https://doi.org/10.1021/jf0400056>.
48. Valko, M.; Leibfritz, D.; Moncol, J.; Cronin, M.T.; Mazur, M.; Telser, J. Free radicals and antioxidants in normal physiological functions and human disease. *Int. J. Biochem. Cell Biol.* **2007**, *39*, 44–84.
49. Nenadis, N.; Tsimidou, M. Observations on the estimation of scavenging activity of phenolic compounds using rapid 1, 1-diphenyl-2-picrylhydrazyl (DPPH<sup>•</sup>) tests. *J. Am. Oil Chem. Soc.* **2002**, *79*, 1191–1195.
50. LeBel, C.P.; Bondy, S.C. Sensitive and rapid quantitation of oxygen reactive species formation in rat synaptosomes. *Neurochem. Int.* **1990**, *17*, 435–440. [https://doi.org/10.1016/0197-0186\(90\)90025-O](https://doi.org/10.1016/0197-0186(90)90025-O).
51. Ali, S.F.; LeBel, C.P.; Bondy, S.C. Reactive oxygen species formation as a biomarker of methylmercury and trimethyltin neurotoxicity. *Neurotoxicology* **1992**, *13*, 637–648.

**Disclaimer/Publisher's Note:** The statements, opinions and data contained in all publications are solely those of the individual author(s) and contributor(s) and not of MDPI and/or the editor(s). MDPI and/or the editor(s) disclaim responsibility for any injury to people or property resulting from any ideas, methods, instructions or products referred to in the content.